Synchrotron X-ray micro-tomography –a new tool for wood identification

(Laboratory of Biomass Morphogenesis and Information)
RISH, Kyoto University

Junji Sugiyama, Mizuno Suyako, Chiori Ito, Yoshiki Horikawa and Misao Yokoyama

Conventional plant taxonomy relies on the characteristics of reproductive organs of plants, though more recently the molecular phylogeny based on DNA analysis is the main stream of the development. Tree- or forest-watching is very popular in these days because of increasing interests to the eco-system. Most of the introductory textbooks follow the classification of flowers, fruits and leaves and allows us to identify plants at species level and sometimes at sub-species level. On the other hand, wood watching is not as popular but professional, and sometimes important in various aspects. Wood identification based on microscopic characteristics has been established and allows us to discriminate wood samples at genus level.

Wood anatomy requires the observation of microstructure from 3 direction, axial, radial, and tangential directions. A way to do is to use a razor blade for making a thin slice from wood blocks, and prepare the microscopy preparation of corresponding 3 directions. Nevertheless this method becomes simple after training and experience, it is not applicable for example when only too small sample is given as is always the case for national heritage class wood works or artifacts. Therefore, we investigated the use of the synchrotron radiation facility(1) to shed a light on the anatomy of national and world heritage wooden objects. X-ray micro-CT imaging at BL20XU (Fig. 1) was carried out on specimens including cultural assets with a resolution of 0.7 micrometer. Sample twig was trimmed less than 1 mm diameter (long along longitudinal axis), and 11 softwood species has been carefully investigated with a series of programs developed by BL20XU, such as SLICE(2). The resolution is good enough to visualize most of the species-specific anatomical features necessary for the identification (for instance Fig. 2), and the work is in progress.

1. Identification of wooden cultural heritage, SPring8, Harima, Hyogo, Japan, project No 2007B15444
2. Tsukasa Nakano, Akira Tsuchiyama, Kentaro Uesugi, Masayuki Uesugi and Kunio Shinohara (2006) Slice – Software for basic 3-D analysis-. Slice Home Page, http://www-20bl.spring8.or.jp/slice/. JASRI.

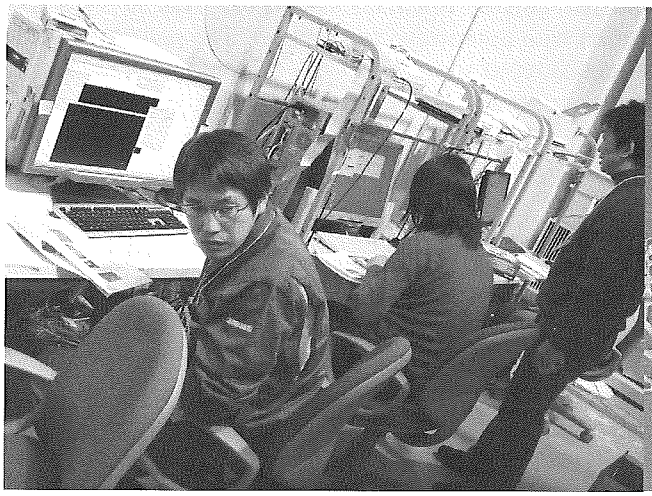

Fig. 1 A snap view of the Experiment at BL20XU.

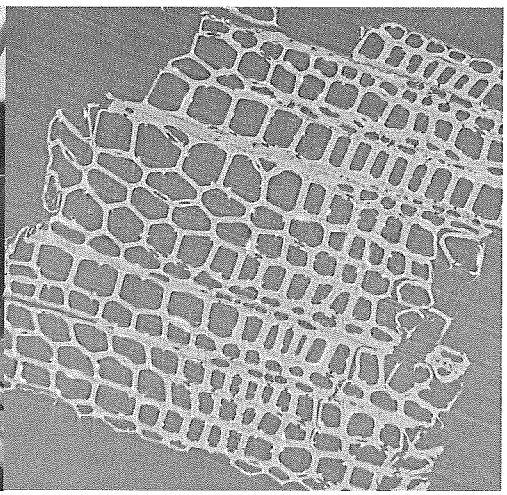

Fig.2 An example of reconstructed slice from ICHII(*Taxus cuspidate*) wood

Lignin Biodegradation by Selective White Rot Fungi as a Biotechnological Tool for Lignocellulosic Biorefinery

(Laboratory of Biomass Conversion, RISH, Kyoto University)

Takashi Watanabe, Takahito Watanabe and Yoichi Honda

Development of conversion systems from lignocellulosics into biofuels and chemicals has received much attention due to immense potentials for the utilization of renewable bioresources. In particular, production of bioethanol from lignocellulosics after saccharification with cellulolytic enzymes is a major concern. Since lignin makes the access of cellulolytic enzymes to cellulose difficult, it is necessary to decompose the network of lignin prior to the enzymatic hydrolysis. Biological pretreatment with white rot fungi in combination with thermochemical or physicochemical treatment is one possible approach for this purpose.

The lignin biodegradation by white rot fungi is an extracellular free radical event that proceeds in concert with the activation of molecular oxygen and redox cycling of transition metals. When wood is colonized by wood degrading fungi, their extracellular enzymes are not able to diffuse into the intact wood cell walls because the enzymes are too large to penetrate the pores of the wood cell walls. Hydroxyl radicals (•OH) are proposed as a principal low molecular mass oxidant that erodes wood cell walls to enhance the accessibility of the extracellular enzymes of wood rot fungi to wood cell wall components. In brown rot, hydroxyl radicals disrupt cellulose and hemicelluloses in wood cell walls, with concomitant modification of lignin substructures. Production of hydroxyl radicals are also reported for non-selective white rot fungi. In the Fenton system, catalysts for the reductive half cycle ($Fe^{3+} \rightarrow Fe^{2+}$) accelerate the hydroxyl radical formation. Wood rot fungi have versatile enzymatic and non-enzymatic systems to accelerate the reductive half cycle. In contrast to brown rot and non-selective white rot fungi, selective lignin-degrading fungi like *Ceriporiopsis subvermispora* are able to decompose lignin in wood cell walls without the intensive damage of cellulose. We first isolated a series of novel itaconic acid derivatives having a long alk(en)yl side chain at position C-3 of its core (ceriporic acids) from the cultures of *C. subvermisrpora*, and showed that ceriporic acids inhibited depolymerization of cellulose by the Fenton reaction, by suppressing a reductive half cycle from Fe^{3+} to Fe^{2+} [1-4]. Wood decay by *C. subvermispora* proceeds without the penetration of extracellular enzymes into the wood cell wall regions. As for the lignin degradation system at a site far from enzymes, lipid peroxidation has been proposed as a major pathway at an incipient stage of wood decay. We analyzed ligninolytic free radical species from hydroperoxides or peroxidizable compounds, and developed several ligninolytic free radical reactions.

The fungal and chemical pretreatments have been applied to various biomass conversion processes. A large scale solid state fermentation of a white rot fungus, *Phellinus* SKM2102 was applied to the pretreatment of Japanese cedar wood, in combination with microwave solvolysis. The pretreatments with white rot fungi were also applied to methane fermentation of wood biomass. The use of white rot fungi and biomimetic radical reactions is attractive not only for increasing saccharification yields but also for decreasing energy input for milling and transportation of the raw feedstock.

REFERENCES

[1] Watanabe, T., Teranishi, H., Honda, Y., Kuwahara, M. (2002) Biochem. Biophys. Res. Commun., 297:918–923.

[2] Rahmawati, N., Ohashi, Y., Watanabe, T., Honda, Y., Watanabe, T. (2005) Biomacromolecules, 6: 2851–2856 (2005).

[3] Ohashi, Y., Kan, Y., Watanabe, T., Honda, Y., Watanabe, T. (2007) Org. Biomol. Chem., 5: 840-847 (2007).

[4] Watanabe, T., Ohashi, Y., Tanabe, T., Honda, Y., Messner, K. (2007) ACS Symposium Series 954, Materials, Chemicals and Energy from Forest Biomass. Am. Chem. Soc. 409-421.

Gene co-expresson network analysis and tropical tree biotechnology

(Laboratory of Metabolic Science of Forest Plants and Microorganisms, RISH, Kyoto University)

Toshiaki Umezawa and Takefumi Hattori

It is becoming more important to establish a sustainable society, which depends on renewable resources. Because wood biomass is the most abundant renewable resource, studies of wood formation is the key to improve forest biomass production. In this context, we are involved in analyzing metabolic functions of forest plants and microorganisms from a wide variety of aspects, including organic chemistry, biochemistry, molecular biology, metabolomics, and systems biology in order to conduct basic investigations contributing cultivation and protection of forest resources. These projects are conducted in collaboration with Dr. Shiro Suzuki, Institute of Sustainability Science, Kyoto University.

1. Gene co-expression network analysis

During the last two decades, significant advances have been made in molecular biology of wood formation. For example, many genes involved in lignin biosynthesis have been cloned and their functions have been unequivocally identified. Having the genes in our hands, the major concern in tree biotechnology is the elucidation of comprehensive gene expression control mechanisms for cell-wall formation. Identification of transcription factors (TFs), as well as microRNAs, controlling expression of genes encoding enzymes involved in cell-wall formation is one of the most important steps. Following the completion of genome sequences of *Arabidopsis thaliana*, a large number of microarray data sets of *A. thaliana* gene expression are open to public, which can be exploited to analyze co-expression of genes. We are conducting gene co-expression network analysis starting with the genes encoding enzymes of the cinnamate/monolignol pathway providing monolignols. This allowed us to find out several genes encoding TFs which possibly control the gene expression of the pathway enzymes. Next, in order to confirm the roles of the TFs, we prepared transgenic *A. thaliana* cells where the individual TF genes were upregulated. Lignin characterization of the transgenic cells thus obtained and *A. thaliana* T-DNA tag line mutants with the target genes being downregulated are under way by the use of Forest Biomass Analytical System, so that we can identify TFs which controls the metabolic flow of the cinnamate/monolignol pathway in *A. thaliana*.

2. Mechanisms for organic acid metabolism of wood-rotting fungi and ectomycorrhizal fungi

Biodegradation of wood components by wood-rotting (WR) fungi including white- and brown-rot basidiomycetes is important as a first process leading to humus production, which in turn contributes greatly to sustainable forest ecosystems. Oxalate excreted from WR fungi plays a wide variety of roles in the degradation owing to its various chemical natures. We have proposed that oxalate metabolism is an important biochemical device to produce energy for fungal growth of WR fungi. Previously, we showed that oxalate is decomposed *via* formate to CO_2 by oxalate decarboxylase and formate dehydrogenase (FDH) during the vegetative growth of the white-rot fungus *Ceriporiopsis subvermispora*. We proposed that his reaction contributed to ATP supply for fungal growth, because FDH also catalyzes the formation of NADH, leading to ATP production. Recently, two cDNAs encoding the FDH were cloned; *CsFDH1* and *CsFDH2*. On the basis of gene expression analysis, *CsFDH1* is strongly suggested to be the main contributor to CsFDH production.

Cytochemical and molecular biological approaches for enzymes and transporters involved in organic acid metabolism are being investigated for WR fungi. Furthermore, comprehensive study for elucidation of regulatory mechanisms for organic acid metabolism in WR and ectomycorrhizal fungi has just begun.

Discovery of the first gene for flavonoid-specific prenyltransferase

(Laboratory of Plant Gene Expression, RISH, Kyoto University)

Kazufumi Yazaki

The prenylation of aromatic compounds is a major contributor to the diversity of plant secondary metabolites due to differences in prenylation position on the aromatic ring, various lengths of prenyl chain, and further modifications of the prenyl moiety, e.g. cyclization and hydroxylation, resulting in the occurrence of more than 1,000 prenylated compounds in plants. Tropical trees are often rich natural resources of those prenylated aromatic compounds. In particular, prenylated flavonoids are reported as being protectants in higher plants to protect them by exhibiting strong antibacterial and antifungal activities, and also recognized as natural compounds that often represent the active components in various medicinal plants and exhibit beneficial effects on human health. In fact, many prenylated flavonoids have been identified as active components in medicinal plants with biological activities, such as anticancer, anti-androgen, anti-leishmania, and anti-NO production. It has been demonstrated that the contribution of prenyl moieties are crucial for these biological activities. However, none of the genes responsible for the prenylation reactions have been identified despite more than 30 years of research in this field.

We have isolated a novel prenyltransferase gene from *Sophora flavescens*, SfN8DT-1, responsible for the prenylation of the flavonoid naringenin at the 8-position, which is specific for flavanones and dimethylallyl diphosphate as substrates [1]. The gene expression of SfN8DT-1 is strictly limited to the root bark where prenylated flavonoids are solely accumulated in planta.

Phylogenetic analysis shows that SfN8DT-1 has the same evolutionary origin as prenyltransferases for vitamin E and plastoquinone. The ectopic expression of SfN8DT-1 in *Arabidopsis thaliana* resulted in the formation of prenylated apigenin, quercetin, and kaempferol, as well as 8-prenylnaringenin. SfN8DT-1 represents the first flavonoid-specific prenyltransferase identified in plants and paves the way for the identification and characterization of further genes responsible for the production of this important class of secondary metabolites.

This achievement was posted by 6 newspapers and several web pages of internet news, as well.

REFERENCES

[1] Sasaki, K., Mito, K., Ohara, K.,Yamamoto, H., Yazaki, K., Cloning and characterization of naringenin 8-prenyltransferase, a flavonoid-specific prenyltransferase of *Sophora flavescens*. *Plant Physiology*, **146 (3)**, 1075-1084 (2008)

Toward intelligent database of geophysical fluid data and beyond: Development of Gfdnavi

(Laboratory of Atmospheric Sensing and Diagnosis, RISH, Kyoto University)

Takeshi Horinouchi

In recent years, scientific data on geophysical and environmental fluids such as the atmosphere and ocean have been increasing explosively. Many data centers and research organizations/groups are now providing data through the Internet, some of which provides on-line visualization capabilities as well. However, once data files are downloaded by users, those server-side services are not available anymore, and they have to handle the data, sometimes in unfamiliar formats, by themselves. Therefore, there are growing needs to search, analyze and visualize data seamlessly across the Internet and desktop by scientists.

In order to reinforce the ability of data management and manipulation in the earth science community (especially in those fields to deal with earth and planetary fluids such as the atmosphere and the ocean), we have been developing a software tool named Gfdnavi (Geophysical fluid data navigator). It is developed under a collaboration of geophysical fluid scientists and database / data-engineering scientists across a number of universities in Japan (Kyoto, Ochanomizu, Kobe, Hokkaido Universities etc.). It is developed as an open source tool and available from the GFD Dennou Club (http://www.gfd-dennou.org).

In Gfdnavi numerical data in different dimensionality and formats are accessed in a consolidated way with an object-oriented library to extract metadata. The metadata are stored in a relational database along with the directory structure, where the metadata of parent directories are inherited downward to child directories. The data and metadata are provided for access with Web browsers for interactive search, analysis, and visualization. A key feature is that the system includes a custom Web server and a metadata scanner, so one can easily start up a service on desktop and use it personally to conduct researches. Yet, it can be operated with widely-used web servers such as Apache to create and operate a data server. The data analysis/visualization user interface is made flexible to support extension. Another unique feature of Gfdnavi is that it can allow users to store derived data and visualization results along with documents and analysis/visualization procedures. Thus, it can not only archive data but also knowledge and methods. To archive data, knowledge, and methods together enables its users to lively reproduce to verify the knowledge and to further apply it.

Gfdnavi is useful to handle data in broader fields rather than just in geophysical fluid sciences. For example, we have demonstrated that it is useful to store and visualize vegetation data. We are planning to enhance its capability to treat image data. We believe that it can be a platform of multi-disciplinary study for the humanosphere if further development is made in this direction.

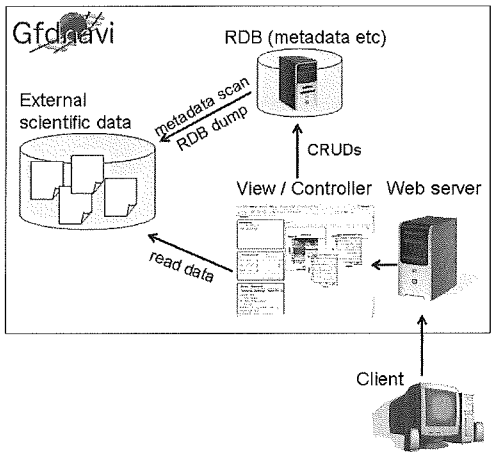

Fig. 1 Overview of the structure of Gfdnavi.

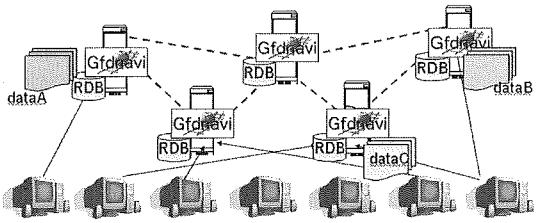

Fig.2 Schematic illustration of the proposed peer-to-pear network of Gfdnavi servers.

Wind observation around tops of midlatitude cirrus clouds by VHF Doppler radar and lidar

(Laboratory for radar atmospheric sciences, RISH, Kyoto University)

Mamoru Yamamoto, Hiroyuki Hashiguchi, and Masayuki K. Yamamoto

Cirriform clouds (cirrus, cirrostratus, cirrocumulus) exist in the upper troposphere consist almost entirely of ice particles, and play a significant role in regulating the radiation balance of the earth-atmosphere system. However, their radiative effects are not sufficiently quantified due to scarcity of observations. Spaceborne and ground-based lidar observations have been carried out to know time and spatial distributions of cirriform clouds and to quantify their microphysical properties. Especially, ground-based lidars are able to observe microphysical properties of cirriform clouds with high time and vertical resolutions.

Dynamical processes are important to understand microphysical processes of clouds. VHF Doppler radars observe height profiles of vertical and horizontal winds by receiving echoes from fluctuations of refractive index and hence have the capability to directly observe them both in clear and cloudy regions. At the Shigaraki MU Observatory, Japan (34°51'N, 136°06'E), Research Institute for Sustainable Humanosphere (RISH), Kyoto University has been operating the VHF (46.5 MHz) Doppler radar named as the Middle and Upper Atmosphere Radar (hereafter MU radar) and Rayleigh/Raman lidar. Because the MU radar is designed to detect very weak echoes in the mesosphere and ionosphere, the MU radar is able to observe wind profiles in the upper troposphere with high time and vertical resolutions. Further, because the lidar installed at Shigaraki is designed to observe vertical profile of temperature up to the mesosphere, the lidar is able to detect tops of cirriform clouds in the upper troposphere. Therefore a combination of the MU radar and the lidar is useful for observing wind motions in and around the cirriform clouds in the upper troposphere.

Figure shows an observational results obtained by the MU radar and the lidar. At several hundred meters above tops of cirrus clouds, eastward wind significantly increased with altitude. Radiosondes launched from the Shigaraki MU Observatory showed that static stability also increased with altitude at several hundred meters above tops of cirrus clouds (not shown). Such wind motions around tops of cirrus clouds has been shown for the first time. Further observations to clarify relations between dynamical and microphysical processes of cirriform clouds will be carried out in the near future.

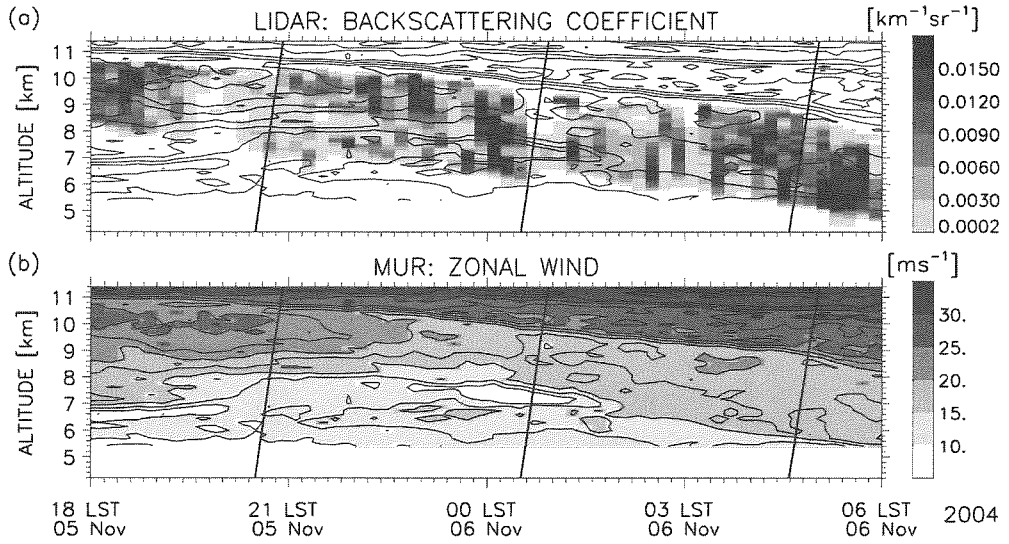

Figure: Shaded areas indicate time-altitude plot of (a) backscattering coefficient observed by the lidar and (b) zonal wind observed by the MU radar from 1800 LST 5 to 0600 LST November 2004. Thin contours indicate zonal wind plotted with 2.5 m s^{-1} intervals. Three thick curves indicate the altitudes of radiosondes.

Cellulose nanofibers from plant sources

Kentaro Abe

Laboratory of Active Bio-based Materials, RISH, Kyoto University

The fabrication of nanofibers, generally defined as fibers with a diameter below 100 nm, is presently the subject of much attention because of their unique characteristics such as a very large surface-to volume ratio and the formation of a highly porous mesh as compared with other commercial fibers. Therefore, these nanofibrous materials are prime candidates for many momentous applications such as reinforcement in nanocomposites, tissue engineering scaffolds, and filtration media. A large number of synthesis and fabrication methods for producing these nanofibers have already been reported. In particular, electrospinning has been the subject of much attention over the past decade.

It is well-known that nanofibers are produced in nature, for example, collagen fibrils in tendons and ligaments and silk fibroin. Among the variety of natural nanofibers, cellulose microfibrils, which are the major constituent of plant cell walls and are also produced by some bacteria, are the most abundant natural nanofiber on earth. The microfibrils, having a width ranging from 5 to 30 nm, are highly crystalline materials formed by laterally packing long cellulose molecules with hydrogen bonding. The resultant stable structure has outstanding mechanical properties, including a high Young' s modulus (138 GPa in the crystal region along the longitudinal direction) and a very low coefficient of thermal expansion (10^{-7} K^{-1} along the longitudinal direction). Therefore, cellulose whiskers and fibrils have great potential for use as reinforcement in nanocomposites and have attracted a great deal of interest recently.

Here we report on an efficient extraction of wood cellulose nanofibers by a very simple mechanical treatment. In cell walls, cellulose microfibril aggregates exist encased by the embedding matrix substances such as hemicellulose and lignin. However, the drying process in typical pulp production generates strong hydrogen bonding between the aggregates after the removal of the matrix, which seems to make it difficult to obtain thin and uniform cellulose nanofibers. Hence we kept the material in the water-swollen state after the removal of the matrix. The undried sample was subjected to a grinding treatment and we obtained cellulose nanofibers with a uniform width of approximately 15nm (Fig. 1a).

This study demonstrates a powerful yet quite simple method for the production of the nanofibers from plant fibers. More stable mass production of the nanofibers can be realized because this method is applicable to other plant sources such as wheat and rice straws (Fig 1b), flax, sugarcane bagasse, and potato pulp (Fig. 1c). We hoped that this result will further stimulate interest in environmentally friendly natural nanomaterials.

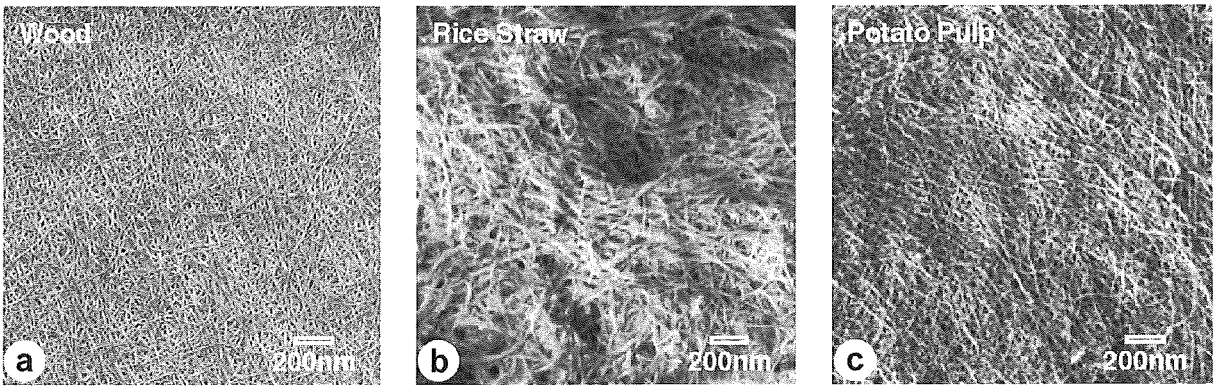

Figure 1. cellulose nanofibers isolated form wood (a), rice straw (b), and potato pulp (c).

Reactivity of Chitosan with Glucose

(Laboratory of Sustainable Materials, RISH, Kyoto University)

Kenji UMEMURA

Chitosan is a deacetylated product of chitin that is extracted from crab and shrimp shells. Recently, chitosan has received attention as a promising biomass resource. As chitosan has an amino group in the chemical structure, chitosan exhibits a polycationic nature. On the other hand, wood is also the most abundant and available biomass resource, and shows generally polyanionic nature. Therefore, they are expected to cause a certain intermolecular interaction and affinity. Research on the interaction of chitosan with wood or wood components has become of interest in recent years. In our laboratory, the interaction of chitosan with wood model compound based on the Maillard reaction has been investigated.

Generally, the Maillard reaction brings the browning of compounds due to the interactions between carbonyl group such as reducing sugars and amino compounds such as amines, amino acids, peptides, or proteins. It is well known that this reaction occurs during the heating, storage, and processing of foods. The Maillard reaction follows a complex mechanism, and the final reaction products yield high molecular weight compounds called melanoidins. The studies on the Maillard reaction between chitosan and reducing sugars are limited and the fundamental information is not yet provided enough. As a recent topic, we introduce the characterization of the Maillard product obtained from the reaction between chitosan and glucose.

Chitosan was dissolved in 1 wt% acetic acid solution, and glucose was added to the chitosan solution. The weight ratios of chitosan and the sugar were adjusted to 10:0, 9:1, 8:2, 5:5, and 3:7. The solutions were stirred at room temperature and then filtered through a filter paper. After removal of air bubbles, the solutions were poured into a small plastic tray and were dried in an oven at 50°C for about 20 h. The films obtained were immersed in an ethanol and 4% sodium hydroxide mixture to remove residual acetic acid and washed thoroughly with an ethanol and distilled water mixture to remove alkali and residual sugar. After the washings showed a neutral pH, the films were vacuum-dried at 50°C for 15 h.

Figure 1 shows the insoluble matter of each chitosan film in 5wt% acetic acid. The insoluble matter increased with increasing glucose addition and then decreased. The maximum value of the insoluble matter recorded was 93% in 20wt% addition. Generally, chitosan is soluble in a dilute acid to form the salt. However, it was demonstrated that chitosan changed easily to insoluble matter by adding glucose. The decrease of the insoluble matter in high addition amount would be due to some acetic acid-soluble substances formed by the Maillard reaction. Figure 2 shows the addition effects of glucose on the tensile properties of chitosan film. The tensile strength steadily increased and then decreased gradually. The maximum average value recorded was 64.8 MPa in 20wt% addition. Compared to pure chitosan film, the tensile strength improved about 45%. Therefore, it was made clear that the insoluble matter to dilute acetic acid and the tensile strength were easily improved by a small amount addition of glucose.

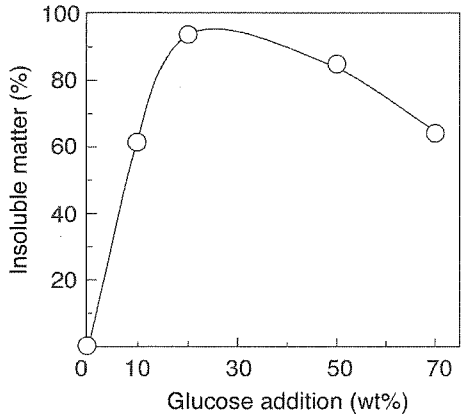

Fig.1. Insoluble matter of the glucose-added chitosan films in 5% acetic acid solution.

Fig.2. Tensile strength of glucose-added chitosan films.

Full-Scale Shaking Table Tests on a Two-Story Wooden Residential House.

Kohei Komatsu, Takuro Mori
(Laboratory of Structural Function, RISH, Kyoto University)

On 8th and 10th January in 2008, a series of full-scale shaking table tests was done on a two-story modern wooden residential house at E-defense, which is well-known as the largest 3D shaking table test facility in the world.

A research team, constituted from RISH, Shinshu University, National Research Institute for Earth Science and Disaster Prevent and a private company which was the sponsor of this full-scale experiment, has been engaging in this big project for almost one year since last summer.

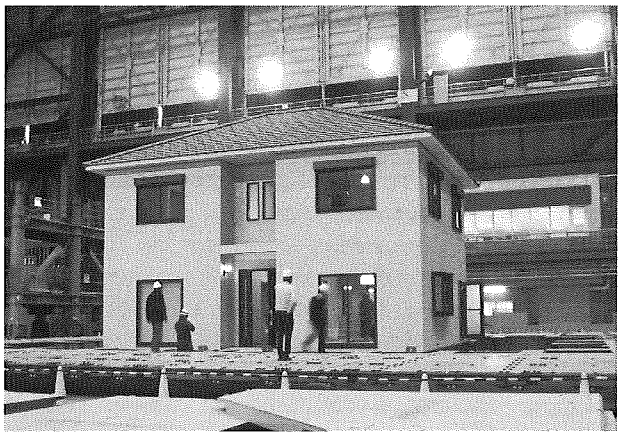

Fig.1. A two-story modern wooden residential house just after the first shaking table test over. Researchers are inspecting damages with a lot of interests (E-defense, Miki, Hyogo prefecture).

Before this full-scale shaking table test, a series of static push-pull cyclic lateral loading tests was conducted on every shear resistant elements, which were expected to give any contributions to the earthquake resisting performance of whole house. Static tests were done by using the common use facilities at Wood Composite Hall in RISH. Not only formal shear walls but also such special elements as hanging wall, bottom wall or even for external sheathing material were evaluated as shown in Figure 2. Figure 3 indicates a comparison between the experimental data observed by acceleration measuring devise on the shaking table at E-defense and predicted behavior of specimen by summing up the performance of all resisting elements involving in the test specimen. It is obvious from this comparison that the modern wooden residential house, which was designed so as to meet with required design criterion, is much stronger and tougher than that of simple prediction.

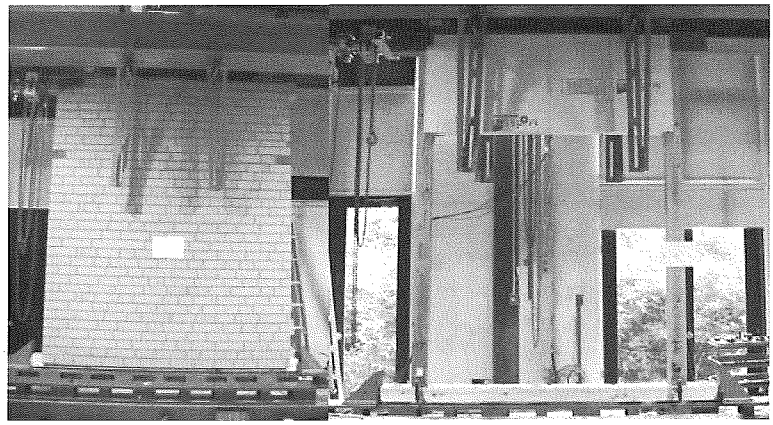

Fig.2. Static push-pull cyclic lateral loading tests on all resisting elements for evaluating their shear resistant performance (Wood Composite Hall, RISH, Uji, Kyoto prefecture)

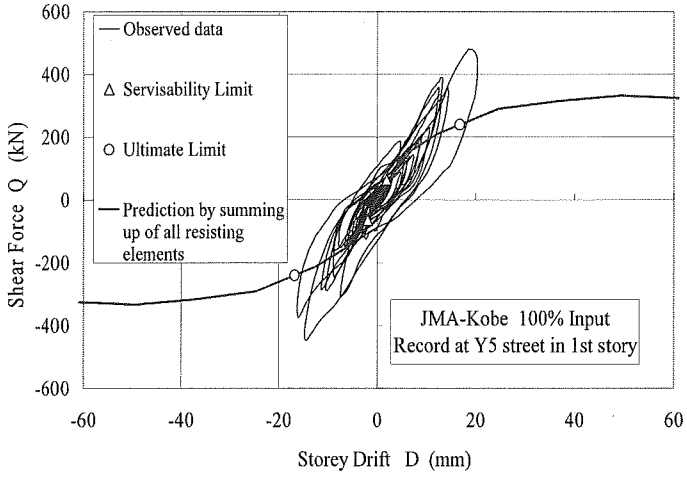

Fig.3 Comparison between observation and prediction.

Acknowledgments: The authors would like to appreciate their special thanks to all graduate students in both universities, for their tremendous contributions to this research project.

A new concept of termite management by the use of non-repellent termiticides

Kunio Tsunoda
Laboratory of Innovative Humano-Habitability, RISH, Kyoto University

We have a long history of combating against termites in Japan since 9th century based on a survey of the literature. Since termites cause considerable economic damage to wooden constructions, they are well recognized as serious urban pests as a result of an increase in the urban population. Among 21 Japanese termite species, *Reticulitermes speratus* (Kolbe) and *Coptotermes formosanus* Shiraki are most economically important subterranean termites.

There are two conventional preventive and control methods to protect wooden houses and structures from termite infestations. One is an industrial/remedial treatment to immunize wood against termite feeding and the other is soil-poisoning to prevent the access of termites to constructions and to control termite infestations as well. Unfortunately, both counterplans are heavily dependent on the use of chemicals. Elimination of the use of chlordane in the 1980's was attributed to an increased public concern about environmental soundness in many countries of the world. Current alternatives generally have a low-mammalian toxicity with a little or negligible environmental impact. Non-repellent termiticides such as imidacloprid, silafluofen, chlorfenapyr, fipronil and other neonicotinoides have been introduced to termiticide-markets. Another development to reduce the risk of soil and water contamination is a physical barrier. Gravels and termite-proof plastic sheeting are good examples of this idea, and were already commercialized in some countries. Although the importance and significance of integrated termite management (ITM) has been often insisted, it has not yet obtained popularity in Japan as in other countries.

The purpose of this short article is to briefly describe the feasibility of a non-repellent termiticide, fipronil in a new concept which is thought to meet requirements as an environmentally sound termite management approach. Non-repellent termiticides may be used as soil-poisoning agents. Nevertheless, we can not expect any favorable environmental contribution accompanied with this application. A bait system would not be applicable to prevention, but enables us to use a small amount of bait toxicants (insect growth regulators instead of termiticides) and to recover residual bait toxicants at the termination of termite management. Characteristics of ecological behavior of termites, grooming and trophallaxis could be taken into consideration in the new concept of termite management with the aid of fipronil.

Transfer of fipronil among workers of Coptotermes formosanus: Laboratory evaluations were conducted at 4 treatment concentrations [0.5-10.0 ppm (m/m)] in sandy loam and two mixing ratios (donors vs. recipients=1:1 and 1:10). After allowing donors (fipronil-exposed workers) to contact with treated sandy loam, they were mixed with recipients (fipronil-unexposed workers) to determine the mortality of both donors and recipients. The final figures for the mortality of donors increased with the treatment concentration and time as expected, and ranged from 30 to 100%, while the mortality of recipients did not vary much with treatment concentrations and mixing ratios with mean figures of 18-36%. The results suggested the possible horizontal transfer of fipronil among nestmates.

Lethal dose of fipronil for workers of Coptotermes formosanus: Lethal dose of fipronil was determined by topical application (0.1, 0.5, 1.0 or 5.0 ng/worker) and contact with treated sandy loam [5 ppm (m/m)]. Topically treated workers of the same dose group were placed in a glass Petri dish (9 cmø) with a water-moistened cotton as a food source for termites to determine LT_{100}s and LT_{50}s based on the change in termite mortality. The LT_{100}/LT_{50} figures were 81/65, 36/24, 27/9, 9/7 hours for 0.1, 0.5, 1.0 and 5.0 ng/worker, respectively. The results clearly supported the dose dependence of fipronil on the termite mortality. The estimated LD_{100}/LD_{50} figures 12 hour-incubation were 2.5 and 2.7 ng/worker. The amount of fipronil recovered from dead termite workers was chemically determined in the contact test for 24 hours. The mean amounts of fipronil recovered were 3.10 and 3.17 ng, respectively from the body exterior and interior with the mean total amount of 6.27 ng fipronil that was much higher than the lethal dose determined by topical application.

Feasibility of a non-repellent termiticide, fipronil in a new concept of termite management: A unit which consists of a container with fipronil-treated soil and termite bait seems applicable to a recoverable, reusable and recyclable devise to eliminate or to suppress foraging activities of subterranean termites in wooden homes and structures. The device requires inspections to confirm whether devices are placed at appropriate sites and to know when the device is renewed, whereas the concept saves labors with an ensured longevity of effectiveness of the device, and should be considered as a part of ITM.

Particle-In-Cell Simulation on the Characteristics of a Receiving Antenna in Space Plasma Environment

(Laboratory of Computer Simulations for Humanospheric Science, RISH, Kyoto University)

Yohei Miyake, Hideyuki Usui, Yoshiharu Omura

For the precise calibration of electric field data obtained by scientific spacecraft, we have to investigate the characteristics of a receiving antenna in space plasma environment. We applied the electromagnetic Particle-In-Cell (PIC) plasma simulation to the antenna analysis in space plasma [1][2]. By using the PIC modeling, we can self-consistently consider the plasma kinetic effects. This enables us to naturally include the effects of the inhomogeneous plasma environment such as a sheath created around the antenna. We particularly modeled situations of electrostatic/electromagnetic-wave reception by an antenna aboard scientific spacecraft and examined the effective length of the antenna.

Fig. 1 shows the model of the current analysis. In the model, we initially set up external waves that propagate in the simulation region. We also placed a wire antenna made of a perfect conductor, in which the electric field values are set to zero. In the simulation, we observed the value of the wave electric field E and the input voltage V_i induced at a gap between two antenna-body elements as shown in Fig. 2. The effective length is obtained as the ratio of V_i / E. In the current study, we examined the effective lengths in receiving the Langmuir and Whistler waves as electrostatic (ES) and electromagnetic (EM) modes, respectively. As a preliminary result, we confirmed that the effective length of the dipole antenna coincides with the half of the dipole physical length in absence of sheath and photoelectron effects. We next started the analysis of a "puck" antenna, which is an electric field instrument for the future satellite mission: BepiColombo. By using a simplified model shown in the bottom panel in Fig. 3, we analyzed the effective length. As a result, the effective length of the "puck" antenna is approximately 80 % of the total length for the simplified model, which is larger than that of a simple dipole antenna [3]. The dependence on the ratio of the sensor length to the boom length and the photoelectron and sheath effects on the effective length should be investigated as a future work.

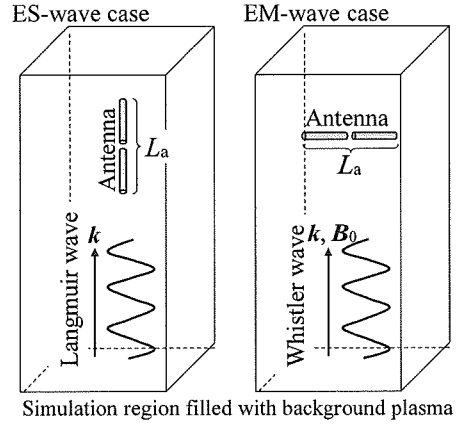

Figure 1. Simulation model for the analysis of receiving antenna characteristics.

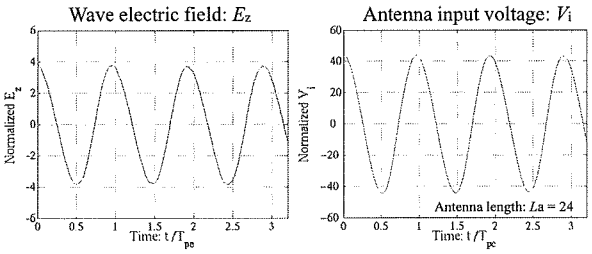

Figure 2. Plasma wave electric field (left panel) and waveform received by a dipole antenna (right panel).

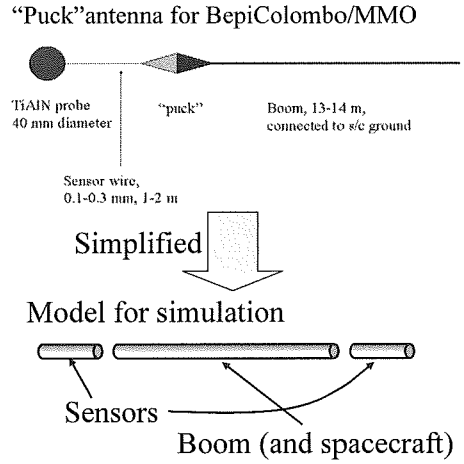

Figure 3. "Puck" antenna (one side, upper panel) and its simplified model for simulation (bottom panel). We set the ratio of the sensor length to the boom length as 1/6.

REFERENCES

[1] Miyake, Y., H. Usui, H. Kojima, Y. Omura, and H. Matsumoto (2008), *Radio Sci.*, 43, RS3004, doi:10.1029/2007RS003707.

[2] Miyake, Y., and H. Usui (2008), *Radio Sci.*, in press.

[3] Miyake, Y., H. Usui, H. Kojima, and Y. Omura (2007), 2007 *AGU Fall Meeting*, San Francisco, USA.

Optimization of uniformly excited phased array and spread spectrum pilot signal for microwave power transmission

(Laboratory of Applied Radio Engineering for Humanosphere, RISH, Kyoto University)

Kozo Hashimoto, Naoki Shinohara and Tomohiko Mitani

1. Uniformly excited phased array

For reduced sidelobes and efficient energy transmission, 10-dB Gaussian tapering, where the energy density of the central part of antenna array is stronger than the edge so that 90% of the output power may be concentrated in the power reception site, has been proposed for its transmitting array antenna for SPS (solar power satellite). This causes a problem on the thermal design since elements at the array center are excited most strongly than those near the edge. Antenna radiation patterns are optimized for high transmission efficiency and low sidelobes under a uniformly excited array in order to solve the problem [1]. The radiation pattern with uniform amplitude excitation for the beam formation subsystem of 12 x 12-element array of SPORTS 5.8 [2] was optimized as a small-scale proof experiment under the assumption that the software retrodirective system will be adopted in a future SPS. The objectives of the multipurpose optimization were to maximize the power in the reception area and to minimize the MSLL (maximum sidelobe level) simultaneously. The radiation patterns that suppress MSLL with high reception power were obtained and the results were experimentally confirmed. The MSLL were suppressed by about 6.6 dB compared with in-phase excitation. It is expected that mutual coupling is hardly influenced when the element interval was 0.6 wavelength in the array antenna element spacing of square patch antennas since the experimental and calculated results matched well as shown in Fig. 1.

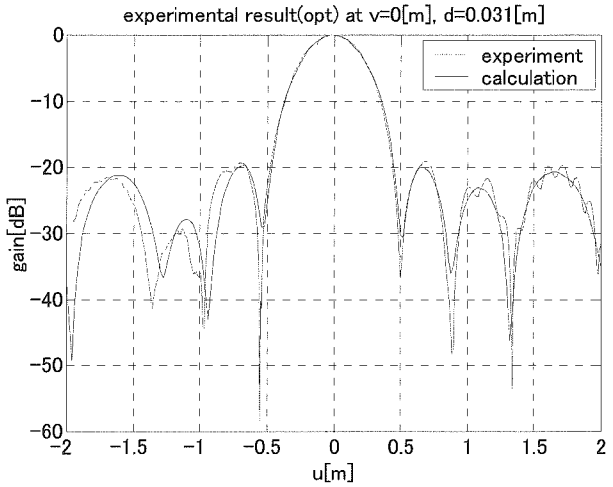

Fig. 1, Example of calculated and experimental phased pattern.

2. Spread spectrum pilot signal

Although the pilot signal without modulation have usually been used in the DOA (direction of arrival) estimation, it has been proven by an experiment that the selection of the multiple pilot signals are possible using the spread spectrum pilot signals and that the frequency of the pilot signal in the same band as the microwave power transmission frequency can be used [3]. Though it had to utilize until now different frequency bands for the energy beam and the pilot signal and two frequency bands became a problem nowadays since the frequency resources are tight. This study shows some hope of solving the problem. In addition, the formation of the microwave power transmission beam to the multiple points was also easy by selecting them using the spread spectrum pilot signals.

References

[1] K. Hashimoto, S. Niijima1, M. Eguchi, and H. Matsumoto, Optimization of uniformly excited phased array for microwave power transmission, International Symposium on Antennas and Propagation 2007, 3B1-2, Niigata, Japan, August, 2007.

[2] Shinohara, N., H. Matsumoto, K. Hashimoto, Phase-Controlled Magnetron Development for SPORTS : Space Power Radio Transmission, The Radio Science Bulletin, 310, 29-35, 2004.

[3] Hashimoto, K., K. Tsutsumi, H. Matsumoto, and N, Shinohara, Space Solar Power System Beam Control with Spread Spectrum Pilot Signals, The Radio Science Bulletin, 311, 31-37, 2004.

Novel Space Environment Monitor, Instrument, and Space Propulsion Systems

(Laboratory of Space Radio Science, RISH, Kyoto University)

Hiroshi Yamakawa, Hirotsugu Kojima, and Yoshikatsu Ueda

1. Monitor system for Space Electromagnetic Environments (MSEE)

The main objective of the MSEE (Monitor system for Space Electromagnetic Environments) is to monitor the electromagnetic disturbances caused by human activities in space. It consists of the small sensor units distributed around the target space (Fig. 1). Our main activities on the development of the MSEE in 2007 are as follows: (a) Development of the analogue ASIC containing the differential amplifiers and A/D converters, (b) Simulation study on the location estimation method for each sensor unit.

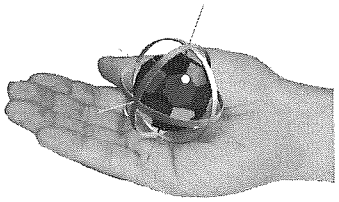

Fig. 1: Sensor unit of the MSEE.

2. Magneto-Plasma Sail (MPS) Space Propulsion System

An MPS (Magneto-Plasma Sail) is a unique propulsion system, which travels through interplanetary space by capturing the energy of the solar wind, which inflates a weak original magnetic field made by a super-conducting coil of about 2-10 m in diameter with an assistance of a high-density plasma jet. From our theoretical estimations, momentum transfer from the solar wind to a spacecraft with a coil is large enough if the plasma source is operated to inflate only the magnetic field away from the spacecraft. Our activities in 2007 are as follows: (a) Sizing (mass, dimension, current, etc.) of the super-conducting coil to produce magnetic field around the spacecraft, (b) Preparation of the experiment facility to measure magnetic field, temperature, current etc. around super-conducting coil.

3. Wave-Particle Interaction Analyzer (WPIA) Instrument for Spacecraft Observation.

Main science target of the WPIA is to detect an energy transfer between plasma wave and plasma particle directly. Generally in collisionless space plasma, wave-particle interaction between plasmas and plasma waves plays much important role of energy exchange. Though direct capture of the interaction was much difficult because of data discontinuity and low time resolution in previous science missions, one of the effective methods is proposed as the interaction measurement between plasma waves and particles. The WPIA which we designed is a new direct calculation system of energy perturbation in space plasma. In the WPIA, we calculate the inner product between electric field and electron particles as following formula in one chip FPGA (Field Programmable Gate Array).

Accessibility and size of *Valonia* cellulose microfibril studied by combined deuteration/rehydrogenation and FTIR technique

Yoshiki Horikawa
(Laboratory of Biomass Morphogenesis and Information)
RISH, Kyoto University

Deuterium has been used as a chemical reagent to estimate the accessibility of cellulose because in organic macromolecules such as cellulose microfibrils, deuterium can replace the hydrogen molecule that comprises the hydrogen bond. In the studies reported in early literature, cellulose specimens were soaked in heavy water (D_2O), and crystallinity was estimated in terms of structural accessibility by calculating the difference in weight (Frilette et al. 1948). With the advent of infrared spectroscopy, accessibility could be estimated by deuteration. Cellulose samples were immersed in NaOD solution for deuteration, washed in D_2O, and dried in a box containing dry nitrogen. Deuterium can be used for infrared spectroscopy because the mass difference due to hydrogen dramatically affects the frequency of molecular vibrations. In cellulose, OD bond vibrations are observed in locations free of other signals. The initial infrared spectrum immediately after exposure of the deuterated specimens to air showed strong OD bands. The intensity of these bands decreased with time due to moisture in the air.

Recently, by high-temperature annealing of the sample at 260 °C in 0.1 N NaOD, the exchange of deuterium was found to occur not only on the microfibril surface but also in the crystalline core (Wada et al. 1997). Despite prolonged exposure of the specimens to air, rehydrogenation occurred only on the surface, while the core remained deuterated.

In this report, we show an FTIR method to measure the accessibility and the size of cellulose microfibrils. This method is similar to the conventional deuteration technique for measuring the accessibility of cellulosic materials; however, the difference in our method is that the hydroxyl groups O2H, O3H, and O6H in the crystalline region were initially completely deuterated. The sample was then rehydrogenated by soaking in water at 25 °C, so that the OD moieties of the crystal surface were rehydrogenated. The ratio of OH to OD absorbance was used to calculate the number of surface vs. core cellulose chains in a microfibril. We applied our novel method to *Valonia* cellulose, whose microfibril have used as a standard sample because of the largest dimensions and high crystallinity.

Hydrogen recovery was considered as a measure of the penetration of hydrogen into the crystal, and it was estimated from the change in OH- and OD-stretching bands. The ratio of absorbance (A) at the OH and OD regions, which are normalized by the absorbance at the CH and CH_2 regions, respectively represents the OD remaining in a sample; R_{exp} (the experimental ratio) is obtained by the following equation:

$$R_{exp} = A_{OD}/(A_{OH} + A_{OD})$$

Cellulose microfibrils consist of numerous linked glucose molecules, each of which exposes 3 hydroxyl groups. It is generally accepted that the cellulose structure has 2 types of H bonds: bonds formed between atoms of the same chain, and H-bonds connecting neighboring chains in the same sheet. O-2-H···O-6 and O-3-H···O-5 links exhibit intrachain H-bonds, while the O-3-H···O-6′ connections exhibit interchain H-bonds (Nishiyama et al. 2002, 2003). Moreover, O-3-H···O-5 bonds were found to be the most stable H-bonds in cellulose. The adjacent oxygen O-2′ in O-6-H···O-3′ interchain H bonds can also serve as an acceptor. All the IR bands in the 3600–3000 cm^{-1} range are O-H stretching mode in alcoholic groups. It is generally accepted that the sharpest band, i.e., that at 3343 cm^{-1}, is assigned to the intrachain H-bond O-3-H···O-5 (Márechal and Chanzy 2000), and that at 2484 cm^{-1} is likely to be an O-3-D···O-5 bond. The R_{exp} value was estimated based on the peaks of these bonds.

As a working model in this study, a microfibril consisting of $p \times q$ chains in a section was considered for simplicity (Figure 1). When deuterated microfibrils are washed in water at 25 °C, only half of the surface ODs is accessible to OH since the other half is buried in the core of the crystalline domain (Figure 1, hatched region). The number of surface chains is $2(p - 1) + 2(q - 1)$, and 2 cellulose chains at the 4 corners are accessible to both sides; therefore, the R_{calc} (the calculated ratio) value at 25 °C is given by the following equation:

$$R_{calc} = \{(p-2) \times (q-2) + (p-1) + (q-1) - 1\} / p \times q$$
$$= (p-1) \times (q-1) / p \times q$$

Assuming that p = 33 and q = 38 (Sugiyama et al. 1984) in the cellulose obtained from *V. macrophysa*, the R_{calc} value was estimated to be 0.943, while the R_{exp} value was 0.934 obtained for the sample washed at 25 °C. This small difference (0.943 vs. 0.934) may be simply because of probable errors of measurements or of more disordered accessible regions in actual sample compared to simple estimation from the surface of cellulose microfibrils. Among organisms that synthesize cellulose, *V. ventricosa* synthesizes cellulose with one of the highest crystallinities; therefore, the microfibrils are closest to the surface/core model assumed for the present formulation, and thus the results agreed quite well.

We devised a stable and reproducible experimental method for accessibility measurement. Therefore, this technique can be applied to a variety of cellulose microfibrils produced by other organisms.

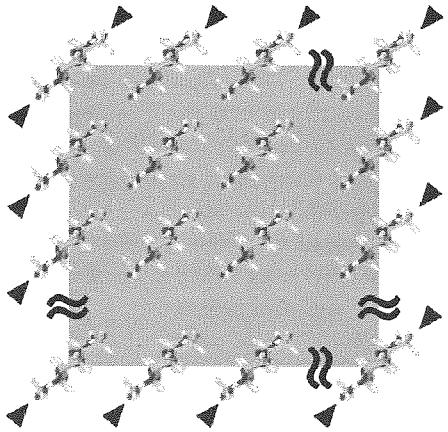

Figure 1 Schematic representation of the cellulose microfibril surface exposed to water at 25 °C after deuteration. The arrowhead indicates the parts of the cellulose chain that are accessible to H.

REFERENCES

[1] Frilette V. J., Hanle J. and Mark H. (1948) Rate of exchange of cellulose with heavy water. J. Am. Chem. Soc. 70: 1107–1113.

[2] Márechal Y. and Chanzy H. (2000) The hydrogen bond network in I-beta cellulose as observed by infrared spectrometry. J. Mol. Struc. 523: 183–196.

[3] Nishiyama Y., Langan P. and Chanzy H. (2002) Crystal structure and hydrogen-bonding system in cellulose I_β from synchrotron X-ray and neutron fiber diffraction. J. Am. Chem. Soc. 124: 9074–9082.

[4] Nishiyama Y., Sugiyama J., Chanzy H. and Langan P. (2003) Crystal structure and hydrogen bonding system in cellulose I_α, from synchrotron X-ray and neutron fiber diffraction. J. Am. Chem. Soc. 125: 14300–14306.

[5] Sugiyama J., Harada H. Fujiyoshi Y. and Uyeda N. 1984. High resolution observations of cellulose microfibrils. Mokuzai Gakkaishi 30: 98–99.

[6] Wada M., Okano T. and Sugiyama J. 1997. Synchrotron-radiated X-ray and neutron diffraction study of native cellulose. Cellulose 4: 221–232.

Studies on a lignin-degrading enzyme of the basidiomycete *Pleurotus ostreatus* using a homologous gene expression system: Oxidation mechanism and molecular breeding of the versatile peroxidase MnP2

Takahisa Tsukihra

Laboratory of Biomass Conversion, RISH, Kyoto University

Lignin is one of the most abundant natural polymers on the earth and a primary component of plant cell walls that confers strength to wood. Lignin forms a matrix surrounding hemicellulose and cellulose, that is the most abundant natural. Lignin is a variable three-dimensional network. Due to its various stable linkages and heterogeneity, lignin is rather resistant to hydrolytic attack and protects the surrounding hemicellulose and cellulose from biological attack by the most microorganisms. However, a certain group of basidiomycetes called white-rot fungi are able to completely degrade lignin to carbon dioxide and water. Thereby, these fungi gain access to the carbohydrate polymers of plant cell walls, which they use as carbon and energy sources. White-rot fungi are also able to degrade toxic aromatic pollutants, because lignin contains a variety of bonds that are commonly present in aromatic pollutants. Therefore, these filamentous wood decaying fungi have a potential application in conversion of lignocellulosic materials to fuels and chemicals, bioremediation for a broad range of environmental pollutants, and biological pulping.

A white-rot basidiomycete, *Pleurotus ostreatus*, secretes a versatile peroxidase (VP), MnP2, which has an extraordinarily wide range of substrate specificity. VP has a substrate spectrum of both of the two common fungal-peroxidase families concerned with lignin degradation, namely, lignin peroxidases (LiP) and manganese peroxidases. Most interestingly, *P. ostreatus* MnP2 oxidizes even high-molecular-weight compounds with high redox potential such as RNase A and a polymeric azo dye, Poly R-478, directly by itself without redox mediators [1]. In *Phanerochaete chrysosporium*, the best studied white-rot fungus, it was reported that Poly R-478 and RNase A were oxidized by LiP only when veratryl alcohol (VA) was present concomitantly in the reaction mixture [2,3]. The purpose of this study is to express a high level of MnP2 in a homologous system and elucidate its oxidation mechanism of high-molecular-weight substrates with high redox potential such as Poly R-478 and RNase A. At first, a molecular breeding approach to isolate P. ostreatus transformants with enhanced productivity of its MnP2 is achieved. Next, with optimization of the culture conditions, hyper-production and exclusive expression of recombinant MnP2 from P. ostreatus is accomplished. The last, MnP2 variants with desired amino acid substitution(s) are produced and their catalytic properties for various substrates are characterized.

Using a DNA-mediated transformation technique [4], a molecular breeding approach to isolate *P. ostreatus* strains with enhanced productivity of MnP2 was achieved. A recombinant *mnp2* construct under the control of *P. ostreatus sdi1* expression signals was introduced into the wild type *P. ostreatus* strain by cotransformation with a carboxin-resistant marker plasmid. A total of 32 transformants containing the recombinant *mnp2* sequence were isolated in a screening with specific amplification by PCR. Productivity of MnP2 in the recombinants was evaluated by the decolorization ability of Poly R-478 on agar plates in the absence of Mn^{2+}. Recombinant *P. ostreatus* strains with elevated MnP productivity were successfully isolated. One of the recombinants, TM2-10, was demonstrated to secret recombinant MnP2 predominantly on a synthetic medium, which was confirmed by RT-PCR and isozyme profile analysis using anion-exchange chromatography. The benzo[*a*]pyrene-removing activity by fungal treatment was analyzed using the isolated recombinant strains, which exhibited enhanced benzo[*a*]pyrene-removing activity. This is the first report to homologously express VP in the basidiomycete. It is demonstrated that *P. ostreatus* strains with enhanced productivity of MnP2 are useful as a biocatalyst, which removes high-molecular compounds and polycyclic aromatic pollutants [5].

Upon optimization of the culture conditions, hyper overproduction of *P. ostreatus* MnP2 was accomplished. Genetically modified *P. ostreatus* strains with the recombinant *mnp2* sequence under the control of *sdi1* expression signals, were subjected to agitated culture using medium supplemented with wheat bran or its hot-water extract. The best result, whereby 7300 U/l of MnP was produced by a recombinant strain TM2-18, indicated that more than 30–fold overproduction of the recombinant MnP2 compared to the above result was achieved. On the other hand, no MnP activity was detected for the wild type strain under the same conditions. Accumulation of the recombinant, but not endogenous, *mnp2* transcripts was demonstrated in reverse-transcription PCR experiments. These results indicated that the

recombinant MnP2 was exclusively expressed by the recombinant strain. Purified recombinant MnP2 showed identical properties to native MnP2 in electrophoresis, spectroscopic and kinetic analyses, including determination of K_m and V_{max} values for Mn^{2+}, H_2O_2 and VA. Moreover, the recombinant MnP2 directly oxidized a high-molecular-weight substrate RNase A in the absence of redox mediators, as does native MnP2. The homologous expression system developed here reflects the post-transcriptional modifications, secretion and stability in the physiological condition during the enzyme production process in *P. ostreatus*. In this context, the system is suitable for analyzing not only the structure-function relationship of the enzyme, but also post-transcriptional regulations in the protein expression pathway of *P. ostreatus*. In addition, the overproduction system will also provide a plat form for exclusive production of mutant or variant peroxidases with desired properties in basidiomycete, because the production of MnP2 in this system is the best results compared to a similar recombinant gene expression system of ligninolytic peroxidases in basidiomycete has been reported [6].

To elucidate the oxidation mechanism of high-molecular-weight substrates by MnP2, a series of mutant enzymes were produced using the homologous gene expression system and their reactivity were characterized. W170A lost drastically the oxidation activity for VA, Poly R-478 and RNase A, while kinetic properties for Mn^{2+} and H_2O_2 were substantially unchanged. These results suggested that, as well as VA, the high-molecular-weight substrates are directly oxidized by MnP2 at W170. Moreover, in the mutants Q266F and V166/168L, amino acid substitution(s) around W170 resulted in a decreased oxidizing activity only for the high-molecular-weight substrates. These results, along with the 3D-modeling of the mutants, suggested that the mutations caused a steric hindrance for access of the polymeric substrates to W170. Another mutant R263N contained a newly generated *N*-glycosylation site and showed higher molecular mass in SDS-PAGE analysis. Interestingly, R263N exhibited an increased reactivity with VA and high-molecular-weight substrates but not with Mn^{2+} and H_2O_2. It was demonstrated that stability at pH 3.0 was increased and higher reactivity at wider pH range compared to wild type MnP2, when Poly R-478 was used as a substrate. On the contrary, with respect to Mn^{2+}- and VA-oxidizing activity, neither the stability at pH 3.0 nor the profile of oxidizing activity at the corresponding pH range was changed by the mutation. Furthermore, the K_m values for Mn^{2+} and VA were almost identical between R263N and wild type MnP2, indicating that recognition of Mn^{2+} and VA were not affected by the mutation. Taking all the observations into account, it is suggested that, in R263N, mode of interaction between the enzyme and the polymeric substrate is slightly changed from that of wild type MnP2, most provably due to the additional *N*-glycosylation. Direct evidence for the possible function of the additional *N*-glycan remains unclear. However, it is expected that, with higher catalytic activity and wider pH stability, R263N can be used for various bio-processes, for example, as an immobilized enzyme in bioreactors for the decomposition of recalcitrant environmental pollutants. It was demonstrated that the homologous expression system provides analysis tools for the effects of post-translational modification on the reactivity of the expressed enzyme. It is noteworthy that the results obtained with R263N could not be gained by using heterologous expression systems. This is the first study on the direct oxidation mechanism for high-molecular-weight substrates by a fungal peroxidase [7].

REFERENCES

[1] Kamitsuji, H., Watanabe, T., Honda, Y. and Kuwahara, M. (2005) Biochem J 386: 387-393
[2] Harvey, P.J., Candeias, L.P., King, P.J., Palmer, J.M. and Wever, R. (1995) Biochem Soc Trans 23: 340S
[3] Sheng, D. and Gold, M.H. (1999) Eur J Biochem 259: 626-634
[4] Honda, Y., Matsuyama, T., Irie, T., Watanabe, T. and Kuwahara, M. (2000) Curr Genet 37: 209-212
[5] Tsukihara, T., Honda, Y., Watanabe, T. and Watanabe, T. (2006) Appl Microbiol Biotechnol 71: 114-120
[6] Tsukihara, T., Honda, Y., Sakai, R., Watanabe, T. and Watanabe, T. (2006) J Biotechnol 126: 431-439
[7] Tsukihara, T., Honda, Y., Sakai, R. and Watanabe, T. (2008) Appl Environ Microbiol 74: 2873-2881

MECHANISMS FOR OXALIC ACID DECOMPOSITION AND TRANSPORT IN WOOD-ROTTING FUNGI

Tomoki Watanabe

Laboratory of Metabolic Science of Forest Plants and Microorganisms,
RISH, Kyoto University

Wood-rotting fungi play an important role in global carbon recycling because they are the major organisms that degrade wood, the most abundant biomass on Earth. Wood cell walls are primarily composed of lignocelluloses, and wood-rotting fungi are grouped into white- and brown-rot fungi on the basis of their ability to degrade this material. White-rot fungi can completely mineralize all wood cell wall components, including lignin. On the other hand, brown-rot fungi metabolize cellulose and hemicellulose without causing depolymerization of lignin [1], although they alter lignin *via* hydroxylation and demethylation [2].

Another biochemical feature that distinguishes the two types of fungi is the amount of oxalate accumulated in culture media. Brown-rot fungi accumulate a large amount of this acid, whereas white-rot fungi do not, but rather decompose it to CO_2 [3, 4].

It is widely assumed that this difference in oxalate accumulation results from different metabolism of oxalate as follows: 1) White-rot fungi degrade oxalate during fungal growth, but most brown-rot fungi do not. 2) Brown-rot fungi possess greater abilities to biosynthesize and transport oxalate than white-rot fungi. However, with regard to 1), the occurrence of both oxalate decarboxylase (ODC, EC 4.1.1.2) catalyzing the conversion of oxalate to formate, and formate dehydrogenase (FDH, EC 1.2.1.2) catalyzing oxidation of formate to CO_2, have never been reported in the same strain of white-rot fungus.

Regarding 2), Munir *et al.* proposed a new concept of oxalate biosynthesis in the wood-rotting basidiomycete *Fomitopsis palustris*. They suggested that oxalate biosynthesis is a fermentation process to acquire energy by oxidizing glucose to oxalate during vegetative mycelial growth [5]. It is essential that oxalate is exported from the cells, because the activities of several indispensable enzymes in the tricarboxylic acid (TCA) and glyoxylate (GLOX) cycles, are inhibited by oxalate [6–8]. However, oxalate transport has not been studied in *F. palustris*.

In this context, it is important to elucidate in detail the mechanisms of oxalate metabolism and transport, to gain insight into the physiological differences between white- and brown-rot fungi.

The first objective of this study is to elucidate the possible role of oxalate decomposition in the white-rot fungus *Ceriporiopsis subvermispora* in relation to fungal growth and lignin degradation.

The author found that *C. subvermispora* possessed two pathways for oxalate decomposition. Each pathway had a different role in this fungus. During vegetative growth, oxalate was decomposed *via* formate to CO_2 by ODC and FDH. It was suggested that this reaction contributed to ATP supply for fungal growth, because FDH also catalyzes the formation of NADH, leading to ATP production. On the other hand, during stationary phase, oxalate was decomposed by oxalate oxidase (OXO, EC 1.2.3.4), which probably supplies H_2O_2 for lignin degradation [9].

FDH of *C. subvermispora*, which was named CsFDH, was purified to clarify its role in oxalate metabolism. This was the first FDH purification from filamentous fungi. Two cDNAs encoding this enzyme were cloned; *CsFDH1* and *CsFDH2*. On the basis of gene expression analysis, *CsFDH1* is strongly suggested to be the main contributor to CsFDH production [10].

The second objective of the present study is to identify an oxalate transporter in *F. palustris*.

A cDNA encoding a protein conferring oxalic acid resistance on *F. palustris* was isolated from the fungus by functional screening of yeast transformants. This cDNA, *FpTRP26* (*Fomitopsis palustris* thioredoxin-related protein 26 kDa), conferred resistance to oxalic acid specifically on the transformant, concomitantly with a decrease in oxalic acid in yeast cells [11]. Furthermore, the author isolated a cDNA from *F. palustris*, *FpOAR* (*Fomitopsis palustris* oxalic acid resistance protein), encoding a membrane protein with oxalate transport activity (Watanabe *et al.* manuscript in preparation).

Based on the results of these studies, different roles of oxalate decomposition and transport between white- and brown-rot fungi are proposed. As shown in Fig. 1, both fungi acquire energy by bicycle mechanisms, in which TCA and constitutive GLOX cycles are essential. In addition to the bicycle mechanism, the white-rot fungus *C. subvermispora* decomposes oxalate to acquire energy and supply H_2O_2 for lignin degradation (Fig. 1A). By contrast, the brown-rot fungus *F. palustris*

efficiently exports large amounts of oxalate, mediated by FpOAR and FpTRP26. The exported oxalate decomposes cellulose yielding the carbon source for fungal growth (Fig. 1B).

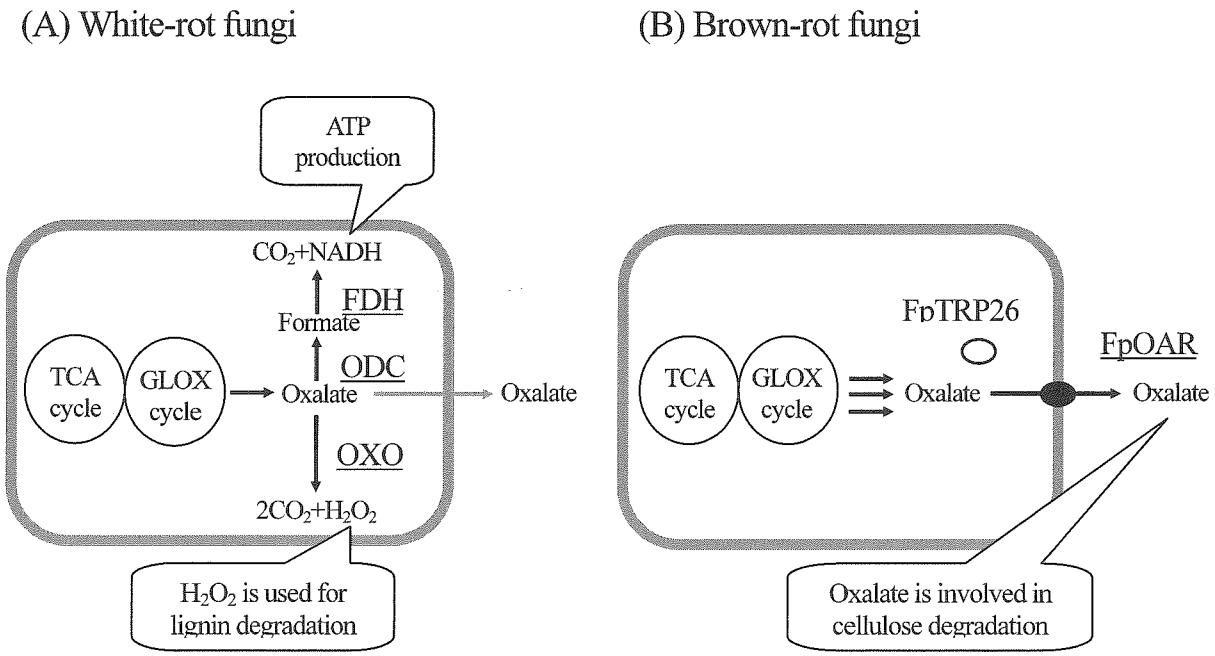

Fig. 1. Possible physiological roles of oxalate decomposition and transport in white-rot fungi (A) and brown-rot fungi (B).

REFERENCES

[1] Crawford, R.L. (1981) Lignin biodegradation and transformation, Wiley, New York, 1-137.
[2] Kirk, T.K., Schultz, E., Connors, W.J., Lorenz, L.R., and Zeikus, J.G. (1978) *Arch. Microbiol.* **117**: 277-285.
[3] Dutton, M.V. and Evans, C.S. (1996) *Can. J. Microbiol.* **42**: 881-895.
[4] Shimada, M., Akamatsu, Y., Tokimatsu, T., Mii, K., and Hattori, T. (1997) *J. Biotechnol.* **53**: 103-113.
[5] Munir, E., Yoon, J.J., Tokimatsu, T., Hattori, T., and Shimada, M. (2001) *Proc. Natl. Acad. Sci. USA* **98**:11126-11130.
[6] Munir, E., Hattori, T., and Shimada, M. (2002a) *Arch. Biochem. Biophys.* **399**: 225-231.
[7] Munir, E., Hattori, T., and Shimada, M. (2002b) *Biosci. Biotechnol. Biochem.* **66**:576-581.
[8] Yoon, J.J., Hattori, T., and Shimada, M. (2003) *Biosci. Biotech. Biochem.* **67**:114-120.
[9] Watanabe, T., Tengku, S., Hattori, T. and Shimada, M. (2005) *Enzyme Microb. Tech.* **37**:68-75.
[10] Watanabe, T., Fujiwara, T., Umezawa, T., and Hattori, T. (2008) *FEMS Microbiol. Lett.* **279**, 64-70.
[11] Watanabe, T., Shitan, N., Umezawa, T., Yazaki, K., Shimada, M., and Hattori, T. (2007) *FEBS letters* **581**:1788-1792.

Functional analysis of ATP-binding cassette proteins involved in nodule formation in legume plants

Akifumi Sugiyama
Laboratory of Plant Gene Expression, RISH, Kyoto University

Legume plants have an ability to fix atmospheric nitrogen into nutrients via symbiosis with soil microbes. As the initial event of the symbiosis, legume plants secrete flavonoids into the rhizosphere to attract rhizobia. The secretion of flavonoids is indispensable for the establishment of symbiotic nitrogen fixation, but almost nothing is known about the membrane transport mechanism of flavonoid secretion from legume root cells. I first performed biochemical analyses to characterize the transport mechanism of flavonoid secretion using soybean (*Glycine max*) and genistein, which is present in the root exudates of soybean to induce *nod* genes of *Bradyrhizobium japonicum*, as a model system.

Plasma membrane vesicles were purified by fractionation of microsomes prepared from soybean roots on a discontinuous sucrose density gradient. Antibodies against plasma membrane H^+-ATPase, vacuolar pyrophosphatase and luminal binding protein were used as markers of plasma membrane, tonoplast, and ER membrane, respectively, in western blot analysis. Plasma membrane vesicles were recovered from the interface of 30 and 40 % sucrose layers. The time course of genistein transport by plasma membrane vesicles was measured. The genistein transport, which was critically dependent on the presence of MgATP, linearly increased up to 15 min incubation. The pH dependency of genistein transport with Tris-Mes buffer ranging from pH 6.0 to pH 9.5 shown its optimum at around pH 8.0, but appreciable activity was observed within the tested pH range. Mechanism of ATP-dependent genistein transport at the plasma membrane vesicles was investigated using various transport inhibitors. Vanadate, a typical inhibitor of ABC transporter acting as a phosphate analogue, inhibited ca. 60 % of the genistein transport, while various ionophores such as gramicidin D, nigericin, or valinomycin did not inhibit the genistein transport (Figure 1). These results suggest the possible involvement of an ABC-type transporter in the secretion of flavonoids from soybean roots [1]. Competition experiments using various flavonoids of both aglycone and glucoside varieties suggested that this transporter recognizes genistein and daidzein, another signaling compound in soybean root exudates, as well as other isoflavonoid aglycones as its substrates. In order to assess whether or not the genistein secretion of soybean roots is induced under nitrogen starvation conditions, transport activity of membrane vesicles from soybean roots grown with or without supplementary nitrogen was compared. Membrane vesicles prepared from plants under nitrogen starvation exhibited a slight, albeit not clearly statistically significant, increase in the genistein transport activity. These findings suggest that transport activity was constitutive regardless of the availability of nitrogen nutrition.

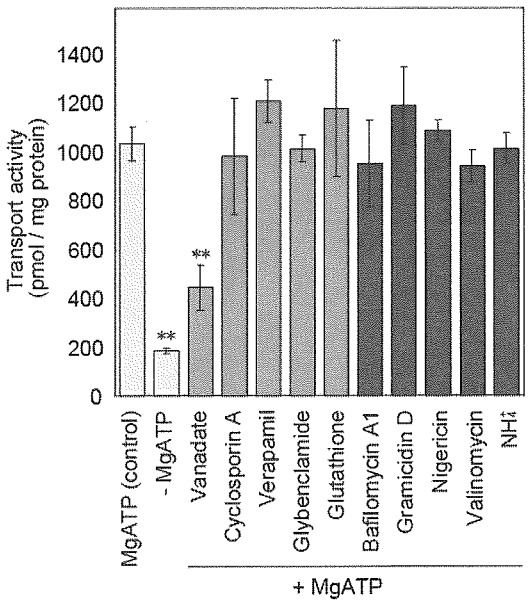

Figure 1. Effects of inhibitors on the genistein transport

Genome-wide analysis of ABC protein genes in a model legume plant, *Lotus japonicus*, was then carried out. For analysis of the *Lotus* genome sequence, a new method "domain-based clustering analysis" was devised, where domain structures like the nucleotide-binding domain and transmembrane domain, instead of full-length amino acid sequences, are used to compare phylogenetically each other. This method enabled to characterize fragments of ABC proteins which frequently appear in a draft sequence of the *Lotus* genome. Ninety-one putative ABC proteins in *L. japonicus*, i.e. 43 "full-size", 40 "half-size" and 18 "soluble" putative ABC proteins were identified (Table 1) [2]. The characteristic feature of the composition is that *Lotus* has extraordinarily many paralogues similar to AtMRP14 and AtPDR12, which are at least six and five members, respectively. Expression analysis of these genes revealed the putative involvement of AtPDR12-like genes in the nodulation process.

Table 1. Comparison of the ABC protein superfamily in plants and humans

	Genome	A	B	C	D	E	F	G	SMC	I	Total	Reference
Lotus	450 Mb	3 (2)	15 (3)	17	2 (1)	1	6	36 (24)	1	10	91	this work
Arabidopsis	125 Mb	17 (16)	27 (5)	15	2 (1)	2	5	44 (29)	4	15	131	3, 4
Rice	440 Mb	7 (7)	28 (4)	17	3 (1)	2	5	51 (30)	4	10	125	5
Human	3000 Mb	12	11 (7)	13	4 (4)	1	3	5 (5)	0	0	49	6

Parentheses indicate the number of half-size ABC proteins for the subfamilies, in which both full- and half-size members are classified as one group.

An AtPDR12-like gene, named LjPDR1, was chosen for further analyses. LjPDR1 is expressed specifically in roots and nodules, and induced by methyl jasmonate. Shoot-applied methyl jasmonate strongly (ca. 800-fold) induced the expression of LjPDR1 in roots. Histochemical analyses with a chimeric gene of LjPDR1 promoter and β-glucuronidase showed the strong expression of LjPDR1 in lateral roots (around the vascular bundles), lateral root primordia, nodule primordia, young nodules, and root tips. Membrane fractioning with sucrose density gradient and aqueous two-phase partitioning system revealed the localization of LjPDR1 at the plasma membrane. These results suggest that LjPDR1function in the nodule formation process mediating the loading of metabolites into vessels or sieve tubes.

REFERENCES

[1] Sugiyama A, Shitan N, Yazaki K (2007) Involvement of a soybean ATP-binding cassette-type transporter in the secretion of genistein, a signal flavonoid in legume-*rhizobium* symbiosis. Plant Physiology. 144: 2000-2008

[2] Sugiyama A, Shitan N, Sato S, Nakamura Y, Tabata S, Yazaki K (2006) Genome-wide analysis of ATP-binding cassette (ABC) proteins in a model legume plant, *Lotus japonicus*: comparison with *Arabidopsis* ABC protein family. DNA Research, 13: 205-228

[3] Sanchez-Fernandez R, Davies TG, Coleman JO, Rea PA (2001) The Arabidopsis thaliana ABC protein superfamily, a complete inventory. J Biol Chem 276: 30231-30244

[4] van den Brule S, Smart CC (2002) The plant PDR family of ABC transporters. Planta 216: 95-106

[5] Garcia O, Bouige P, Forestier C, Dassa E (2004) Inventory and comparative analysis of rice and Arabidopsis ATP-binding cassette (ABC) systems. J Mol Biol 343: 249-265

[6] Dean M, Rzhetsky A, Allikmets R (2001) The human ATP-binding cassette (ABC) transporter superfamily. Genome Res 11: 1156-1166

An observational study of ozone variation in the tropical tropopause layer

Hisahiro Takashima
Laboratory of Atmospheric Environment Information Analysis, RISH, Kyoto University

Space-time variations of ozone in the topical tropopause layer (TTL) are investigated using ozonesonde data. Because the TTL is an entry point from the troposphere to the stratosphere for air mass and chemical species which affect stratospheric air conditions, it is important to understand tracer distributions in the TTL and related stratosphere-troposphere exchange (STE) processes. However, atmospheric measurements including trace gas observations have not been extensively conducted around tropical regions.

To understand the physical processes in the TTL, ozone variations with seasonal and intra-seasonal time scales have been investigated by paying particular attention to the longitudinal structure. There are very few papers focusing on the zonal variations of ozone and temperature simultaneously in the TTL. This is partly because ozonesonde observations in the tropics have not been extensively conducted in both space and time. Since attention is focused on rather shallow structures of ozone and temperature around the tropopause, a 5-year ozonesonde data set at nine stations around the tropics from the Southern Hemisphere Additional Ozonesondes (SHADOZ) archive [1] was used. The longitudinal ozone distribution in the tropical upper troposphere (TUT) shows a zonal wave number one structure with maxima around the Atlantic and Africa, and minima around the western Pacific throughout the year, while the annual variation shows maxima during northern summer to autumn at most longitudes. The ozone distribution was compared with the vertical temperature structure, and it was found that the lapse rate is gradual (steep) at the ozone-enhanced (reduced) longitude and season. The east-west temperature structure and ozone variation in the TUT can be explained by the longitudinal variation of large-scale atmospheric responses to the tropical heat source.

A warm anomaly in the middle and upper troposphere (below 355 K potential temperature level) and a cold anomaly near the tropopause are observed over the convectively active region with an eastward tilt of the temperature structure above the 355 K level. At the same time, low ozone air mass in the marine boundary layer (MBL) reaches above the 355 K level with rapid upwelling motion. Ozone variability in the TUT is also large around the Atlantic and Africa and small around the western Pacific. However, the zonal wave one structure is not clear in the temperature variability and in the correlation coefficient between ozone and temperature, which can be related to wave activities around the tropopause. Remarkably large ozone variabilities with good correlation are observed in Africa during summer and in the central Pacific during autumn-winter. These could be associated with large scale equatorial waves, but the longitudinal variation of the wave activities does not seem to be an important factor in the zonal wave one structure of ozone.

Because the data gap in the SHADOZ archive still exists in the tropical central Pacific, seasonal variations of ozone at Christmas Island (2°N, 157°W) have been investigated using observations conducted as a part of the SOWER (Soundings of Ozone and Water in the Equatorial Region) /Pacific mission [2]. At Christmas Is., one of those SOWER bases in the equatorial central Pacific (Figure 1), ozone and water vapor observations had been conducted in nine campaigns from 1999 to 2003. This is a very unique location since it is far from polluted air source and there has been no such observation in the equatorial central Pacific. Anticyclonic circulations in the upper troposphere in relation to the large-scale atmospheric responses to the tropical heat source are located around the eastward of the large scale convective area and the westward of Christmas Is. Throughout the year, ozone concentration at Christmas Island is low with small ozone variation in the whole troposphere particularly in the MBL with ~10 ppbv near the surface (Figure 2). Just below the tropopause substantially reduced ozone concentrations (<10 ppbv) similar to those found in the MBL were observed during the August 2002 campaign, which is maintained at least during the observation period. From meteorological conditions, we found that air mass was advected from the Inter-Tropical Convergence Zone (ITCZ) located to the north of Christmas Island in accordance with the northeasterly wind that is only observed during northern summer in the upper troposphere.

Though at Christmas Island ozone and temperature variability in time is rather small with low ozone concentration, systematic variations in ozone and water vapor around the tropopause associated with a convectively coupled equatorial Kelvin wave were observed during June 2002 campaign. The structure around the tropopause satisfied a dispersion relationship for an equatorial Kelvin wave in linear theory, and

ozone and water vapor variations similar to those presented in a previous study [3] are observed. The ozone and water vapor variations associated with this wave event are small, but it could play an important role in the tracer distributions and the STE processes even during northern summer.

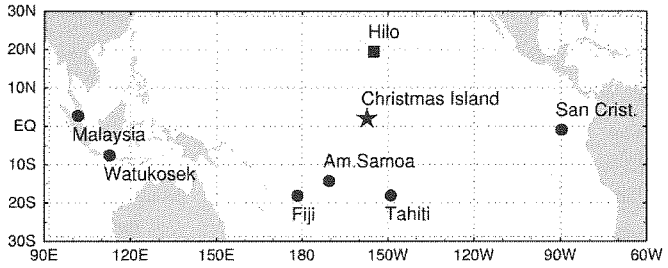

Figure 1. Locations of the tropical Pacific ozonesonde station from SHADOZ (circle), and that of Hilo (square) and Christmas Island (157◦W, 2◦N) (star).

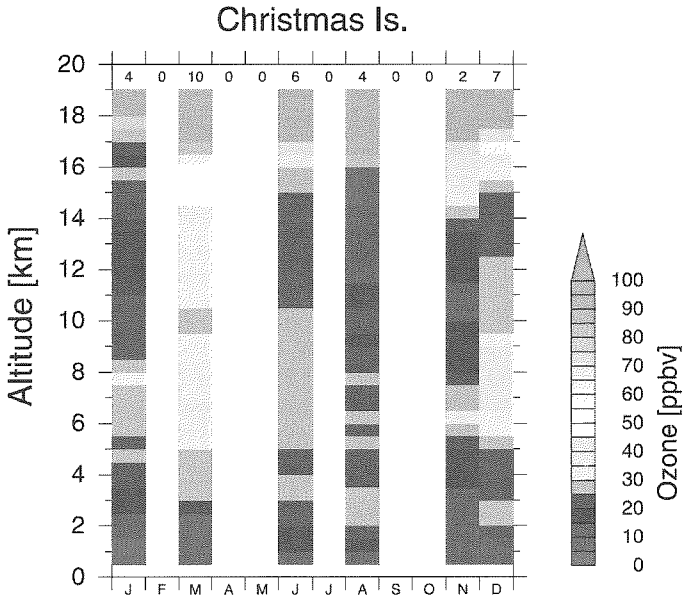

Figure 2. Vertical distributions of ozone mixing ratio (ppbv) for each month averaged in 0.5 km bins at Christmas Island. The number of observations for each month is shown in the upper part of this figure.

REFERENCES

[1] Thompson, A. M., et al. (2003) J. Geophys. Res. 108: 8238, doi:10.1029/2001JD000967

[2] Hasebe, F., M. Fujiwara, N. Nishi, M. S. H. Voemel, S. Oltmans, H. Takashima, S. Saraspriya, N. Komala, and Y. Inai (2007) Atmos. Chem. Phys. 7: 803–813

[3] Fujiwara, M., F. Hasebe, M. Shiotani, N. Nishi, H. Voemel, and S. Oltmans (2001) Geophys. Res. Lett., 28 (16): 3143–3146

Space-time variability of equatorial Kelvin waves and intraseasonal oscillations around the tropical tropopause

Junko Suzuki
Laboratory of Atmospheric Environment Information Analysis, RISH, Kyoto University

Recently some research efforts have been focusing on the tropical tropopause layer (TTL) where dynamical and chemical properties of the atmosphere gradually change from tropospheric to stratospheric features [1]. They have been conducted mostly from the view point of stratosphere-troposphere exchange (STE), since the TTL is the primary exchange region of mass and chemical species between the troposphere and the stratosphere. In particular for water vapor, temperature variation in the TTL is one of the most important factors to control the dehydration mechanism of air entering the lower stratosphere from the upper troposphere. The Kelvin wave and the intraseasonal oscillation (ISO) are dominant variations around the tropical tropopause. In spite of their importance in variations around the TTL, seasonal and longitudinal characteristics of the Kelvin wave and the ISO have not been clearly documented yet. Using the European Centre for Medium-Range Weather Forecasts (ECMWF) 40-year reanalysis data for the period September 1957 through August 2002, seasonal and longitudinal variations of the Kelvin waves and ISOs in temperature and zonal wind around the tropical tropopause are investigated. The outgoing longwave radiation (OLR) data for the proxy of deep convections are also examined because of their possible influence on the dynamical fields in the TTL.

The space-time spectral analysis was first performed for the temperature and zonal wind fields around the tropical tropopause, and two dominant spectral regions in the eastward propagating domain are found: one for Kelvin waves with zonal wavenumbers from 1 to 10, periods from 4 to 23 days and equivalent depths from 8 to 240 m and the other for ISOs with wavenumbers from 1 to 10 and periods 23 to 92 days. To investigate space-time variability of Kelvin waves and ISOs we reconstructed the grid data for the two spectral windows through the Fourier forward and inverse transforms, and calculated the square amplitude at each grid point. We mostly focused on the zonal wind field, because the vertical structure in zonal wind is less variable than that in temperature; consequently the results for zonal wind seem to be unaffected by the seasonality around the tropical tropopause particularly seen in the temperature field. Kelvin wave activities in zonal wind are vigorous during two seasons, one in January to March and the other in June to August around the upper troposphere up to 100 hPa. In contrast, there is a clear difference in the maximum longitude (Figure 1); at 100 hPa it is located in the eastern hemisphere from the Indian Ocean to the western Pacific, but at 150 hPa and below it is located in the western hemisphere from the eastern Pacific to the South America. To further investigate a relation to deep convection as a source of these disturbances we calculated activities in the OLR data for the Kelvin wave spectral window. Then we found that the activities in OLR do not correspond to those in zonal wind, suggesting that the Kelvin wave activity in zonal wind may not necessarily depend on convection.

As to the change in the maximum altitude of Kelvin wave activities in the upper troposphere we refer to the climatological background zonal wind which is easterly in the eastern hemisphere and westerly in the western hemisphere. Kelvin waves in the westerly region possibly suffer damping when the background zonal wind is getting close to the zonal phase speed. In such a condition the group velocity slows down, and the zonal wind amplitude is increasing. On the contrary in the eastern hemisphere, the amplitude of Kelvin waves propagating vertically in the easterly can increase, because of sudden increase in the Brunt-Väisälä frequency N [2]. Another point to note at 100 hPa is that the maximum Kelvin wave activity is large in the westward of the maximum easterly wind. It would be due to distortion or dissipation of Kelvin waves propagating into the active convective region which is located around the maximum easterly.

The ISO activities in zonal wind at 100 hPa are seen in the western Pacific during northern winter, which are somewhat larger than those of the Kelvin waves. For this spectral window the ISO activities in zonal wind and OLR are related with each other, indicating that the eastward moving disturbance with the ISO timescale is somehow coupled with the organized convective system such as the Madden-Julian oscillation (MJO).

The lifecycle of Kelvin waves is further investigated in relation to background wind and convective activity. To pick up Kelvin wave events we set the threshold as the easterly component with -1σ at each height (e.g., -2.79 m s^{-1} at 100 hPa). The total number of extracted Kelvin waves is over 3000 for 45 years. The Kelvin wave amplitudes do not show large difference in longitude, but Kelvin wave events can be seen

in a specific region at each height, which is closely related to Figure 1: at 100 hPa the waves mostly appear around 15°W - 60°E and disappear around 15°E - 120°E; at 200 hPa they appear around 150°E - 90°W and 75°W - 0 °, and disappear 180° - 45°W and 60°W - 45°E, respectively.

From the composite analysis the Kelvin waves appearing around 165°E - 125°W at 200 hPa seem to be generated by latent heat energy released from deep convection over the Indian Ocean and the western Pacific (Figure 2-A). These waves propagate eastward through the westerly wind and decrease their amplitudes. After that, weak signals still continue to propagate with acceleration over the South American Continent. At 100 hPa the Kelvin waves appearing around 15°W - 60°E seem to be generated in the convective region over the South American Continent, and the signals propagate eastward and get into another convective region which is located over the African continent or the Indian Ocean and western Pacific Ocean (Figure 2-B). To the west of the South American Continent, the signals could be traced upstream: some waves found at 200 hPa could propagate up to the 100 hPa-level (Figure 2-A'). The OLR and easterly wind anomalies propagate eastward in phase around the appearance region: the convectively coupled Kelvin waves are included in these waves found at 100 hPa over the Indian Ocean and the western Pacific (Figure 2-C).

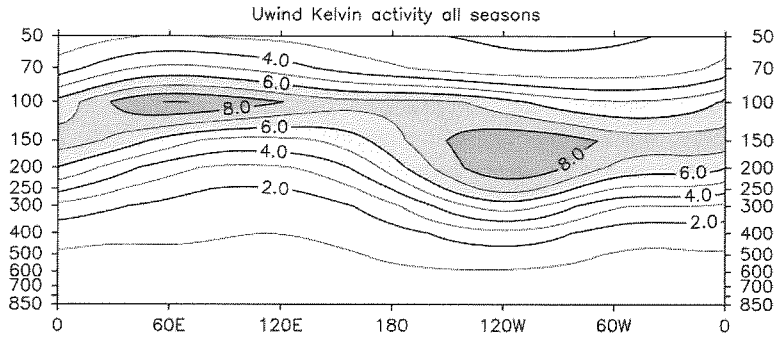

Figure 1: Longitude-height section of the annual mean Kelvin wave activities of zonal wind. A contour interval is 1.0 m^2 s^{-2}, and shading begins above 4.0 m^2 s^{-2}.

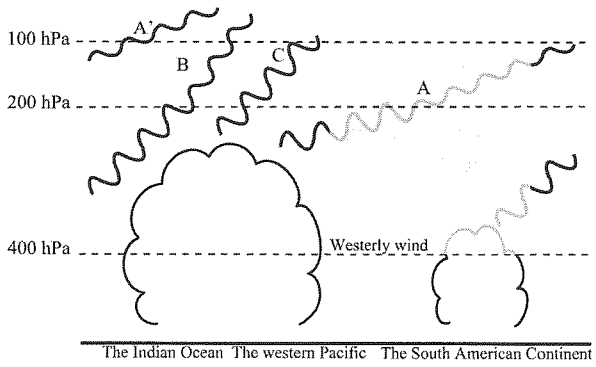

Figure 2: Schematic longitude-height diagram illustrating the source and passing through regions of Kelvin wave. Wavy lines represent Kelvin waves. Shading represents the westerly region. Letters of A (A'), B and C are described in the text.

REFERENCES

[1] Highwood, E. J., and B. J. Hoskins (1998), *Q. J. R. Meteorol. Soc.*, *124*, 1579-1604.

[2] Shiotani, M., and T. Horinouchi (1993), *J. Meteorol. Soc., Jpn.*, *71*, 175- 182.

NANO-FIBRILLATION OF WOOD PULP FOR THE UTILIZATION IN OPTICALY TRANSPARENT NANOCOMPOSITES

Shinichiro Iwamoto
Laboratory of Active Bio-based Materials, RISH, Kyoto University

Cellulose is a linear polymer consisting of D-anhydroglucose units joined together by β-1,4-glycosidic linkages. All plants and some kinds of animals, fungi, and algae produce cellulose, as far as we know. In the wood cell wall, cellulose molecular chains form fibrous structures called microfibrils that are 3 to 4 nm wide. Due to the stable structure of their crystalline regions, microfibrils show high mechanical properties along the longitudinal direction, such as a Young's modulus close to 138 GPa [1] and an estimated strength of at least 2 GPa, based on experimental results for kraft pulp. Furthermore, measurement of the coefficient of thermal expansion (CTE) of all cellulose composites indicates that the CTE of microfibrils is as small as that of quartz, at 0.1 x 10^{-6} $°C^{-1}$ [2]. These singular features make cellulose microfibrils and related nanofibers prospective candidates for reinforcement in nanomaterials.

Mechanical reinforcement of optically functional materials is of significant interest to various industries. Nanocomposite materials with less than one-tenth of a wavelength in size are free from light scattering, making cellulose nanofibers a promising candidate for reinforcement of transparent materials. Yano *et al.* [3] demonstrated that bacterial cellulose (BC) nanofibers sized 50 x 10 nm in cross-section can reinforce acrylic and/or epoxy resin without losing their transparency at a fiber content of 60 %. Furthermore, they showed that the nanocomposites exhibit a low CTE of 6 x 10^{-6} $°C^{-1}$ (as good as of glass), high strength of 325 MPa, comparable to that of soft steel, and ease of bending similar to that of plastics. Optically transparent nanocomposites are highly suitable for use in electronic devices such as flexible display substrates. However, utilization of BC is limited compared to plant based-nanofibers because of their low productivity. Therefore, the reinforcement of optically transparent plastics by plant based-nanofibers, the most abundant resources on Earth, is highly desirable.

The objective of this study is the development of optically transparent composites using wood pulp nanofibers as reinforcement. Wood pulp is several tens micro-meter wide fiber, consisted of aggregates of 3 to 4 nm wide cellulose microfibrils comprising a multi–layered structure with hemicellulose and lignin as a matrix between the microfibrils. Therefore, the utilization of the pulp as reinforcements of optically transparent composites requires the nano-fibrillation of the pulp into microfibrils or their bundles with several tens nano-meter width. Nano-fibrillation procedures using a high-pressure homogenizer and a grinder were investigated. Then, to optimize the nano-fibrillation treatment, the effect of the treatment conditions on the mechanical and thermal properties of the optically transparent composites was investigated. Finally, to improve the process of nano-fibrillation for the production of optically transparent nanocomposites with high mechanical properties and low thermal expansion, the effects of hemicellulose content on pulp were investigated in terms of the aggregation of microfibrils.

The fibrillation procedures of wood kraft pulp into nano-sized wide fibers were compared using a high-pressure homogenizer and a grinder [4]. The high-pressure homogenizer treatment was not sufficient to achieve uniform nano-fibrillation. On the other hand, repetition of the grinder treatment after the high-pressure homogenizer treatment did fibrillate pulp into uniform nanofibers. To optimize the grinder treatment for the processing of optically transparent composites, the effects of the fibrillation conditions on the physical properties of the composites were investigated [5]. The dissolved pulp was subjected to various passes through the grinder. The fibrillated pulp gradually turned into uniform 20 to 50 nm wide fibers after up to 5 passes through the grinder. The light transmittance at 600 nm wavelength of the fibrillated pulp composites reached 80 %. However, further passes did not change the size of the fibrillated pulp and the light transmittance of the composites. In addition, as the number of passes through the grinder increased, the fibrillated pulp was subjected to degradation, which can be explained by the decrease in the degree of crystallinity and the degree of polymerization of the cellulose. The degradation of the fibrillated pulp led to a decrease in the mechanical properties and an increase in the thermal expansion of the sheets and composites. Thus, it was concluded that the production of high-performance optically transparent nanocomposites requires a reduction in the number of passes in nano-fibrillation using a grinder.

To reduce the number of passes, the effects of hemicellulose content on pulp were investigated in terms of the aggregation of microfibrils [6]. Four types of pulps: never and once-dried holocellulose

pulp with and without alkali treatment were prepared. The mild alkali treatment removed hemicelluloses from holocellulose pulp. Regardless of the presence of hemicelluloses, irreversible hydrogen bonding against rewetting occurred due to drying in the pulps. With the single-pass grinder treatment of the pulps, the never and once-dried holocellulose and never-dried alkali-treated pulps were fibrillated into 10 to 20 nm-wide fibers, while the once-dried alkali-treated pulp did not achieve nano-fibrillation, indicating that hemicelluloses serve as inhibitors of the coalescence of microfibrils, contributing to the ease of nano-fibrillation.

In addition, the coefficient of thermal expansion (CTE) values of the fibrillated never and once-dried holocellulose pulp sheets and composites were extremely low, at approximately 8 and 10 x 10^{-6} $°C^{-1}$, respectively; these values were about one-eighth of that of acrylic resin. The fibrillated never and once-dried alkali-treated pulp composites had higher CTE values than the fibrillated never and once-dried holocellulose pulp composites. With respect to mechanical properties, the fibrillated never and once-dried holocellulose pulp composites showed remarkable results with a Young's modulus of approximately 16 GPa and a strength of about 280 MPa, exhibiting higher figures than those of the fibrillated never and once-dried alkali-treated pulp composites. These results indicate that hemicelluloses play a role in adhesion between nanofibers, contributing to the thermal stability, stiffness and strength of composites.

In conclusion, 10 to 20 nm wide nanofibers which are thinner than BC were obtained from wood pulp (Fig. 1). Furthermore, the optically transparent nanocomposites exhibiting a light transmittance of 83 % at 600 nm wavelength, a coefficient of thermal expansion of 10 x 10^{-6} $°C^{-1}$, Young's modulus of 16 GPa, and tensile strength of 280 GPa were obtained at a fiber content of 85 wt% using wood pulp nanofibers as reinforcement.

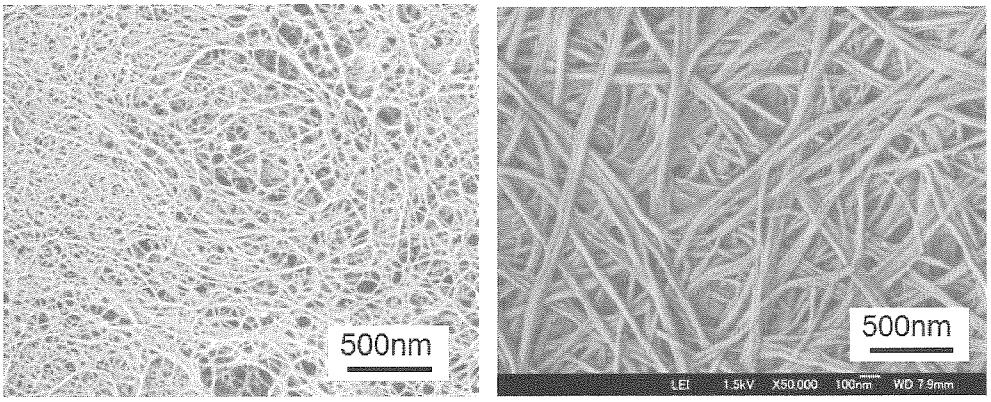

Figure 1. Scanning micrographs of (a) wood pulp and (b) Bacterial cellulose nanofibers.

1.Sakurada, I. *et al.*, *Journal of Polymer Science*, 1962. **57**(165): p. 651-660.
2.Nishino, T. *et al.*, *Macromolecules*, 2004. **37**(20): p. 7683-7687.
3.Yano, H. *et al.*, *Advanced Materials*, 2005. **17**(2): p. 153-155.
4.Iwamoto, S. *et* al., *Applied Physics A: Materials Science and Processing*, 2005. **81**(6): p. 1109-1112.
5.Iwamoto, S. *et al.*, *Applied Physics A: Materials Science and Processing*, 2007. **89**(2): p. 461-466.
6.Iwamoto, S. *et al.*, *Biomacromolecules*,2008. **9**(3): p. 1022-1026.

Properties of Non-Wood Plant Fiber Bundles and the Development of Their Composites

Sasa Sofyan Munawar

Laboratory of Sustainable Materials, RISH, Kyoto University

Among the natural fibers obtained from annual non-wood plant fibers. In order to promote some plant fibers and to develop their composites, it is necessary to understand their mechanical properties. The mechanical properties of plant fibers depend on their physical, chemical, and morphological properties, such as fiber orientation, cellulose content, crystal structure and diameter/cross-sectional area of the fiber. The fiber cross-sectional area strongly influences to the evaluation of fiber strength [1]. To establish the procedure for determined of fiber cross-section area, the evaluation of the reliability of diameter measurement of fiber bundles by using optical microscope is needed. However, the methods used for determining the fiber cross-sectional area have not been fully exploited.

In recent years, chemical, thermal and physical treatments had been used for fiber surface treatment. Alkali solution and steam refining process had been used for the treatments [2][3], while only cotton fiber has been coated by chitosan solution to improve their properties [4]. However, the investigations of mild steam treatment with low temperature and steam pressure, and chitosan coated plant fiber have not been exploited.

On the other hand, the steam pre-treated exploded Miscanthus sinensis with the low temperature and steam pressure showed higher mechanical properties of binderless fiberboard than that of high temperature and steam pressure of pre-treatment [5]. However, the utilization of long fiber bundles treated with mild steam and layered with different orientation on mats have not been fully exploited.

The objectives of this study were to evaluate the method of measuring the cross-sectional area as parameter to determine of mechanical properties of plant fiber bundle. Then, the fibers were treated with alkali, mild steam and chitosan treatment to improve their properties. The oriented boards were manufactured with steam treated fibers using hot pressing system.

In order to evaluate the method for measuring of fiber cross sectional area; abaca, pineapple, sansevieria, sisal, coconut, kenaf and ramie fiber bundles from Indonesia were used as materials. The cross-sectional area of each fiber bundle was observed using a scanning electron microscope (SEM). The coefficient factor as parameter to evaluate the method of measuring cross-sectional area is defined as the ratio of the cross-sectional area determined from a representative SEM image (Sr) selected for each fiber by image analysis software, to the cross-sectional area of each fiber determined by using the circle equation (Sc) based on average value of five locations diameter measurement by using optical microscope (So).

The coefficient factor of fiber cross-sectional area was in the range of 0.92-0.96. The values of Sc shows to evaluate 4-8% lower values than those of Sr. Thereby, the coefficient factors of each fiber have little influence to evaluate So. Based on the result, So has been used directly for the determination of fiber strength [6]. In addition, ramie, pineapple and sansevieria fibers provide higher values of the average tensile strength than other fibers i.e. 849 MPa, 654 MPa and 562 MPa, respectively.

Therefore, ramie, pineapple and sansevieria fibers were treated by alkali, mild steam and chitosan solution to improve their properties. The fibers were immersed in a NaOH solution of 2% (w/v) at 95°C for 2h for alkali treatment, while for mild steam treatment; the fibers were steamed by using boiling water in the screen-covered bath at steam pressure about 0.1 MPa for 2h. In addition, the fibers were immersed to 4% and 8% chitosan solution at room temperature for 2h. Degree of crystallinity, crystallite size and crystallite orientation of fibers were determined by x-ray diffraction method.

The fiber after steam treatment showed the higher value of degree of crystallinity than untreated and alkali treatment. The steam treatment for all fiber provided a higher value of crystallite orientation than untreated and alkali treated fibers. It was observed that the steam treatment for all fibers gave slightly higher value of crystallite size than untreated and alkali treated fibers. Alkali and steam treatments remove a certain amount of wax and oils covering the external surface of the fibers and its surface become slightly smoother than untreated fiber, and the monofilament can be visible. On the other hand, the chitosan 4% was more uniformly covered on the fiber surfaces than the chitosan 8%. Steam-treated and chitosan 4%-coated ramie fiber provides higher values of the average tensile strength than other

fibers i.e. 892 MPa and 875 MPa, respectively. The decrease in tensile strength and Young's modulus of alkali treated fibers was probably due to the decrease in the degree of crystallinity and crystallite orientation [7]. In addition, high water absorption causes the swelling of cellulose fibers, resulting poor mechanical properties. This fact also may attribute to fiber damage.

Furthermore, in order to utilize the steam-treated ramie, pineapple and sansevieria fibers, each fiber were used on board manufacturing. Phenol–formaldehyde resin solution was chosen for impregnation and adhesive purposes. The uni-oriented direction (0° fiber orientations) board and cross-oriented direction (90° fiber orientations) board developed from the untreated and mild steam-treated fibers with a target density of 800kg/m^3.

The result showed that the internal bond of oriented boards increases when the fibers treated with mild steam. The high internal bond was 1.33 MPa for uni-oriented steam-treated sansevieria board and the lowest one was 0.45 MPa for cross-oriented untreated pineapple board. The boards made from steam-treated fibers provided higher properties in modulus of rupture (MOR) and modulus of elasticity (MOE). The uni-oriented boards showed higher average values of MOR and MOE compared to cross-oriented boards. The high values of MOR and MOE were 403 MPa and 39.2 GPa for uni-oriented steam-treated sansevieria boards (Fig. 1). The differences for board MOR and MOE were found mainly due to the differences on the ratios of fiber substances on board to density of fiber bundles [8]. Based on the results of this study, when the ratios of fiber fraction to fiber density are one, it was calculated that: the values of the MOR parallel to the fibers of the uni-oriented boards without adhesives reach 80% of the fiber's strength. Mild steam treatment of fibers imparts the dimensional stability of boards. The dimensional stability of steam-treated boards has been increased compared to untreated board.

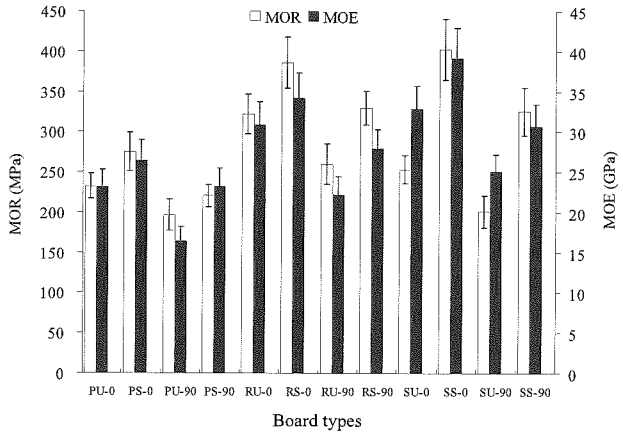

Fig. 1. MOR and MOE parallel to the fiber of the boards. PU-0, uni-oriented untreated pineapple board; PS-0, uni-oriented steam-treated pineapple board; PU-90, cross-oriented untreated pineapple board; PS-90, cross-oriented steam-treated pineapple board; RU-0, uni-oriented untreated ramie board; RS-0, uni-oriented steam-treated ramie board; RU-90, cross-oriented untreated ramie board; RS-90, cross-oriented steam-treated ramie board; SU-0, uni-oriented untreated sansevieria; SS-0, uni-oriented steam-treated sansevieria; SU-90, cross-oriented untreated sansevieria; SS-90, cross-oriented steam-treated sansevieria.

REFERENCES

[1] Bledzki AK, Gassan J (1999) Prog Polym Sci 24:221–274
[2] Mohanty AK, Misra M, Drzal LT (2001) Compos Interfaces 8:313-343
[3] Xu J, Widyorini R, Yamauchi H, Kawai S (2006) J Wood Sci 52:236–243
[4] Liu XD, Nishi N, Tokura S, Sakairi N (2001) Carbohydr Polym 44:233–238
[5] Velasquez JA, Ferrando F, Farriol X, Salvado (2003) Wood Sci. Technol. 37: 269-278
[6] Munawar SS, Umemura K, Kawai S (2006) J Wood Sci 53:108-113
[7] Munawar SS, Umemura K, Tanaka F, Kawai S (2007) J Wood Sci 54(1): 28-35
[8] Munawar SS, Umemura K, Kawai S (2008) J Wood Sci (DIO: 10 . 1007/s10086-008-0968-2)

Formation Mechanism of Microstructure in carbonized wood

Kengo Ishimaru

Laboratory of Innovative Humano-habitability, RISH, Kyoto University
(Present: Central Research Laboratory, Daiwa House Industry Co., Ltd.)

Carbon materials are classified by graphite-related and diamond related carbon materials. The former is composed of stacking hexagonal carbon layers based on sp^2-bonded carbon atoms; the latter consists of sp^3-bonded carbon atoms involved in tetrahedral bonds. Microstructure of graphite-related carbon materials such as a carbonized wood consists of mainly carbon crystallites, cross-linking between them, and oxygen-containing functional groups. The mechanical, electronic, and structural properties of the graphite-related carbon materials depend mainly on the three-dimensional arrangement of the carbon crystallites forming the carbon skeleton. The recent developments in wood-based carbon materials provide new application fields for the new functions of carbonized wood [1, 2], while at the same time demonstrating the necessity of finding a way to control its microstructure. The further development of various wood-based carbon materials requires that the carbonization process of wood and the formation mechanism of the microstructure of carbonized wood be sufficiently clarified, and that their microstructure on the nano scale be fully controlled. In the present study, the formation mechanism of the microstructure of carbonized wood was investigated systematically, focusing on the carbonization behavior and microstructural change in the carbonization process between 500 and 1800°C of Japanese cedar by spectroscopic and microscopic analysis. As a result, new interesting information was found with respect to the microstructure and its formation process in the wood carbonization. The details are summarized as follows.

Firstly, the carbonization behavior of wood at the early stage of the carbonization process between 500 and 1000°C is discussed in detail by comparison with that of cellulose and lignin [3]. A carbon crystallite composed of polyaromatic carbon planes in carbonized-wood, -cellulose, and -lignin was formed due to the decomposition and volatilization of non-aromatic functional groups up to 600°C. The degree of ordering of carbon crystallites at each heat treatment temperature is described in the ascending order of carbonized-lignin, -wood, and -cellulose. This could be due to differences among carbonized-wood, -cellulose, and -lignin in the degree of cross-linking, such as ether bridges and disordered aromatic structures, in the range of 500-600°C. It appears that the degree and process of carbon crystallites' development of carbonized wood are closer to those of carbonized cellulose than to those of carbonized lignin. This suggests that the degree of development of the carbon crystallites and the cross-linking for carbonized-wood, -cellulose, and -lignin during carbonization are closely related to the O/C atomic ratio before carbonization. Byrne and Nagle have proposed a cellulose microfibril dominance model for the formation mechanism of carbonized wood microstructures [4]. The present results prove that the microstructure in carbonized wood is strongly affected by the composition ratio of carbon to oxygen atoms in the raw wood.

Secondly, structural changes of sp^2-bonded carbons as the main carbon skeleton of carbonized wood between 500 and 1800°C was studied by XPS, Raman, XRD, and TEM [5]. The results of the spectroscopic analysis of carbonized wood showed that the microstructure of carbonized wood changes drastically at approximately 1400°C. The XPS and Raman results proved that the degree of disorder in carbon crystallites decreased significantly from 800 to 1400°C with decomposing of the cross-linkings such as oxygen-containing functional groups and amorphous phase sp^2-bonded carbon up to 1400°C. XRD results showed that the plane size of the hexagonal carbon layer in a carbon crystallite increased mainly up to 1400°C, and the number of the hexagonal carbon layers in a carbon crystallite increased significantly above 1400°C. TEM observation of wood carbonized at 700 and 1800°C visually showed that its predominant structure was turbostratic, and carbon crystallites approximately 1 nm in size at 700°C grew up to about a 3 to 10 nm size at 1800°C. The growth of the carbon crystallites was observed clearly above 1400°C.

Sp^3-bonded carbon of the sub-microstructural component in wood carbonized from 700 to 1800°C was qualified by Raman and TEM analysis [5]. The TEM results showed the existence of an onion-like and nano-diamond structure based on sp^3-bonded carbons in wood carbonized at 700°C, which suggested that the carbon structure of wood at the early stage of carbonization is a complex of various allotropic carbon structures [6, 7]. Nano-diamond based on sp^3-bonded carbon would be formed by the reaction between

sp^3-bonded carbon and volatilized oxygen atoms in carbonized wood at a low temperature of 700°C. The Raman spectra of carbonized wood proved that part of the microstructure in carbonized wood from 700 to 1800°C was made of the combination of sp^2- and sp^3-bonded carbon. Since sp^3-bonded carbon is the rigid cross-linking of carbon crystallites, the microstructure of carbonized wood could be highly disordered. It was found that the sp^3-bonded carbons were transformed from an amorphous to nanocrystalline structure with the growth of carbon crystallites in the temperature range above 1400°C. The structural development of rigid cross-linking of sp^3-bonded carbon would disturb the well-ordering of carbon crystallites in the high heat temperature range above 2000°C.

Finally, the microstructure in the cell walls of wood carbonized from 700 to 1800°C was clarified on the basis of the results of TEM observation and pinpoint Raman analysis [8]. The discrete layers in the cell walls of the raw wood were no longer observed at 700°C. SEM- and TEM-observations confirmed that the microstructure in a cell wall for carbonized wood was turbostratic in nature without any heterogeneity originating from the constitutional heterogeneity of wood. However, well-ordered carbon crystallites were observed on the inner surface of a cell wall for a sample carbonized at 1800°C. This surface layer could be formed by deposition of vaporized carbon gasses on the surface of cell walls during heat treatment, and may play an important role in the formation of the preferred orientation of carbon crystallites and multi-phase graphitization of carbonized wood at high temperatures [9].

On the base of the concerns mentioned above, the microstructural control in carbonized wood could be applied to the development of various wood-based carbon materials. As one possibility, the microstructure on the nano scale of carbonized wood would be controlled by the adjustment in quantity of sp^3-bonded carbon as cross-linkings of carbon crystallites. For the development of wood catalytic graphitization, carbonized wood, containing less amount of sp^3-bonded carbon, should be used as a carbon precursor because sp^3-bonded carbon disturb the well alignment of carbon crystallites as cross-linking during graphitization. On the other hand, for the addition of more stiffness to SiC and SiC/C composites, carbonized wood, including a large amount of sp^3-bonded carbon, should be utilized as a raw material in order to increase the number of the edge of carbon crystallites where silicon atoms react to carbon atoms. As another possibility, the microstructure between the inner surface and inside of the cell walls of carbonized wood would be controlled by the change of the permeability of volatized gases into cell lumen. By the development of well alignment carbon layers on the inner surface of cell walls of carbonized wood, it has heterogeneous microstructure between the inner surface and inside of cell wall. Such carbon materials are available to be as solid cathode batteries such as an electric double layer capacitor and lithium ion battery. Thus, the microstructural control in carbonized wood could be applied to the development of various wood-based materials, and be broadened the utilization of them as carbon materials.

REFERENCES

[1] Fujisawa, M., Hata, T., Bronsveld, P., Castro, V., Tanaka, F., Kikuchi, H. and Imamura, Y., J. Eur. Ceram. Soc., 2005, 25, 2735-2738

[2] Hata, T., Ishimaru, K., Fujisawa, M., Bronsveld, P., Vystavel, T., Hosson, JD., Kikuchi, H., Nishizawa, T. and Imamura, Y., Fullerene Nanotube Carbon Nanostr., 2005, 13, 435-445

[3] Ishimaru, K., Hata, T., Bronsveld, P. and Imamura, Y., J. Mater. Sci., 2007, 42, 122-129

[4] Byrne, CE. and Nagle, DC., Carbon, 1997, 35, 267-273

[5] Ishimaru, K., Hata, T., Bronsveld, P., Nishizawa, T. and Imamura, Y., J. Wood Sci., 2007, 53, 442-448

[6] Hata, T., Imamura, Y., Kobayashi, E., Yamane, T. and Kikuchi, K., J. Wood Sci., 2000, 46, 89-92

[7] Ishimaru, K., Vystavel, T., Bronsveld, P., Hata, T., Imamura, Y. and Hosson, JD., J. Wood Sci., 2001, 47, 414-416

[8] Ishimaru, K., Hata, T., Bronsveld, P. and Imamura, Y., J. Mater. Sci., 2007, 42, 2662-2668

[9] Otani, S. and Oya, A., Tanso, 1971, 64, 10-13 (in Japanese)

Development and characterization of shape-controlled porous-carbon by flash heating of wood biomass

Fumio Kurosaki

Laboratory of Innovative Humano-habitability, RISH, Kyoto University

The utilization of carbonized wood biomass has recently received fresh impetus owing to the vast amount of waste wood that has to be recycled without posing an environmental hazard. In particular, the use of carbonized wood biomass as a source of advanced carbon materials is been gaining considerable attention because of its high porosity and surface area. However, shape-controllability and pore distributions of porous carbon materials are also very important factors that determine its practical utility in industrial production [1,2]. Wood biomass maintains the original cell structure after carbonization, and its macro-textural cannot be changed easily. In the case of conventional heating, wood is converted into carbon by a series of chemical reactions such as dehydration, depolymerization [3]. On the other hand, flash heating means very rapid heating treatment for raw materials and the heating rate is defined 10-1000 °C /sec. The mechanism of thermal conversion is not the same for conventional or slow heating and flash heating. Flash heating of wood biomass promotes the depolymerization of starting materials in carbonization, e.g. fragmentation leading to a large quantity of volatiles evolving during the process [3].

The porosity determines the ability of fluid passage and treatment on porous carbons [4], and the surface area determines the reactivity and capacity in each application. Generally, finer carbon-particle sizes are effective for increasing the surface area. However, such fineness brings about a decrease in the porosity between the particles. Furthermore, shape control of porous carbons requires many additional processes such as granulation, heat treatment, and compression. Recently, shape-controlled porous carbon (SC-PC) materials and their simple and inexpensive preparation methods have been applied in advanced technological fields such as catalyst filters [5], fuel cell batteries [6], and functional porous metals [7].

Firstly, flash heating has been applied for the liquefaction of wood biomass [3] and a semi-closed graphite-reactor has been used to realize unique macro-texture and shape controllability in this study. Flash heating very effectively changed the original micro-texture of the sawdust into a texture similar to that of melted carbon [8], and it was also reported that the shapes of the carbon products after flash heating corresponded to the interior shape of the semi-closed graphite-reactor [9]. The shape-controlled porous-carbon synthesized by flash heating in the semi-closed graphite-reactor showed a porosity of over 80%, which originated from the macro-pores (size: 5–50 μm) between cross-linked carbon beams. Moreover, such three-dimensional macro-texture also enables shape control of porous carbons without binders or frames and provides versatility in manufacture, design, and finishing (Fig. 1). However, the BET surface area of the SC-PC was found to be 370 m^2/g, which is half the surface area of conventional activated carbon powder [10].

The surface area of carbon materials increases with oxidation on the surface of a precursor; this process is called activation. Activation has been applied widely in industry because the oxidation facilitates the development of micro-pores and meso-pores. Then, secondary, the SC-PC prepared by flash heating of sawdust in a semi-closed graphite-reactor system was improved by a subsequent heat treatment. This new porous carbon products combined a high surface area of 670m^2/g with high porosity of over 80%. Subsequent low-temperature heat treatment (380 °C) was effective in increasing the surface area while maintaining the original three-dimensional microtexture and porosity. In addition, the heat treatment produced meso-pores of between 5 nm and 50 nm and micro-pores of less than 2 nm on the surface of the cross-linked carbon beams that formed the shape of the carbon material (Fig. 2). Moreover, macro-pores of between 5 μm and 50 μm were observed between the crosslinked carbon beams. Therefore, it was confirmed that shape-controlled multi-porous carbon (SC-MPC) contained micro-, meso-, and macro-pores in its microtexture while retaining its shape and strength [10].

Finally, a catalyst filter that deposited Pd-nano-particles homogeneously was synthesized by using SC-MPC as a novel catalyst support and by employing an electroless-plating procedure. In addition, SC-Ni was obtained by electrically plating nickel on SC-PC and subsequently removing the SC-PC as a carbon template. The surfaces of SC-MPC-Pd and the SC-PNi were analyzed and the modifications for application to advanced materials were determined by using electrical microscopes, porosimeters, XRD, and XPS. The Pd particles had sizes smaller than 5 nm and they were distributed homogeneously on the amorphous

carbon surface and reduced to metallic Pd particles in SC-MPC (Fig. 3). SC-PNi was obtained from cross-linked nickel tubes and its chemical composition mainly showed metallic nickel (Fig. 4) [10]. These syntheses can be tailored easily to produce other catalyst filters containing nano-particles of various noble metals, and porous metals such as Pt, Au, Ag, Cu, and Pd. Thus, SC-MPC has potential for wide utilization in various industrial fields such as environmental cleaning, electronic devices, and enzyme containers.

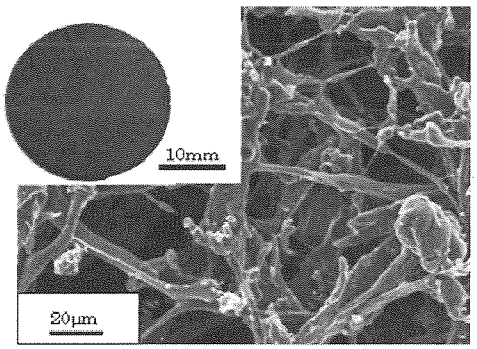

Fig. 1. Appearance and microtexture of coin shaped SC-PC prepared by flash heating and semi-closed reactor system.

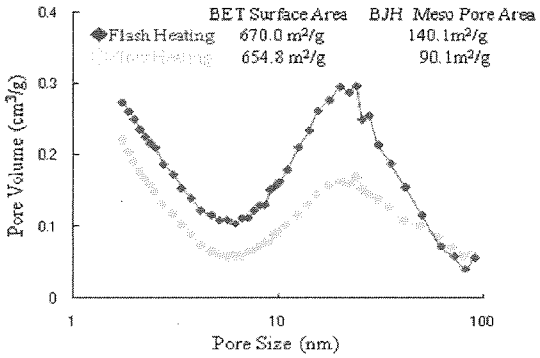

Fig. 2. dV/dlogD meso-pore volume distribution of the SC-MPC and activated slow heating sample.

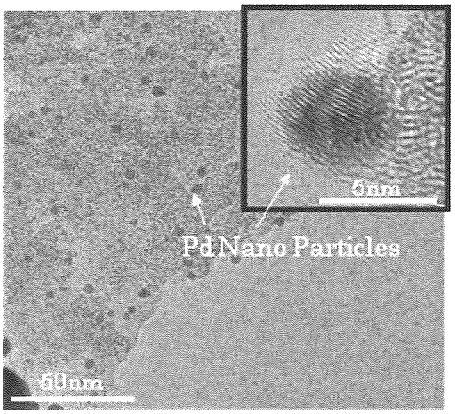

Fig. 3.The distribution of Pd and high resolution image of the Pd nano particle on the amorphous carbon surface observed by TEM.

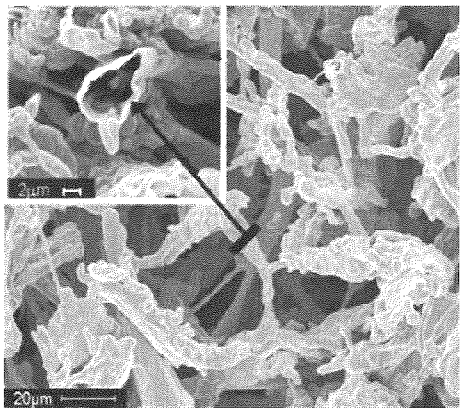

Fig. 4. The macro-texture of the surface and the cross-section on the cross-linked nickel tubes observed by SEM.

REFERENCES

[1] Rios R. V. R. A., Martinez-Escandell M., Molina-Sabio M., and Rodriguez-Reinoso F. Carbon, 2006, 44, 1448-1454.
[2] Calvo M., Garcia R., Arenillas A., Suarez I., and Moinelo S. R., Fuel, 2005, 84, 2184-2189.
[3] Graham R. G., Bergougnou M. A., and Overend R. P., J. Anal. Appl. Pyrol., 1984, 9, 95-135.
[4] Brasquest C. and Cloirec P. L., Carbon, 1997, 35, 1307-1313.
[5] Auer E., Freund A., Pietsch J. and Tacke T., Appl. Catal., 1998, A173, 259-271.
[6] Moriguch I., Nakahara F., Furukawa H., Yamada H., and Kudo T. Electrochem. Solid-State Lett. 2004, 7, A221-223.
[7] Banhart J. Manufacture, Prog. Mater. Sci. 2001; 46:559–632.
[8] Kurosaki, F. Ishimaru, K., Hata, T., Bronsveld, P., Kobayashi E. and Imamura Y., Carbon, 2003, 41, 3057-3062.
[9] Kurosaki F., Koyanaka H., Hata T. and Imamura Y., Carbon, 2007, 45, 671-673.
[10] Kurosaki F., Koyanaka H., Tsujimoto M. and Imamura Y., Carbon, 2008, 46, 850-857.

Development of a New Analytical Method for Quantifying Benzalkonium Chloride in Treated Wood and Evaluation of its Leaching Characteristics under Different Ambient Conditions

Teruhisa Miyauchi

Hokkaido Forest Products Research Institute, Nishikagura 1-10, Asahikawa, Hokkaido 071-0198, Japan
(Research fellow, Laboratory of Innovative Humano-habitability)

Type-1 ammoniacal copper quaternary (ACQ-1) wood preservatives, which comprise copper and benzalkonium chloride (BAC) as active ingredients [1] are among the most widely used wood preservatives for pressure treatment in Japan as alternatives to chromated copper arsenate (CCA) wood preservatives [2]. BAC in ACQ-1 comprises homologues having different alkyl chain lengths (C12, C14, and C16 homologues), which possess different physical, chemical, and microbiological properties. Thus, it is important to elucidate the leaching characteristics of each BAC homologue in order to guarantee the protection of wood and to improve the performance of ACQ-1-treated wood. Furthermore, it is also important to eliminate the effects of environmental factors on the leaching of each BAC homologue from treated wood in order to improve the performance and extend the applications of ACQ-1-treated wood.

To investigate the leaching characteristics of each BAC homologue, a quantitative determination method was required, which could be used to quantify each BAC homologue in treated wood. Thus, during the first stage of this study, a method involving high-performance liquid chromatography with ultraviolet detection (HPLC-UV) and solid-phase extraction (SPE) was developed for the quantitative determination of each homologue in treated wood [3-5]. This method is applicable for the inspection of treated wood in keeping with official standards.

Next, by using the method developed, the leaching characteristics of the BAC homologues and the environmental factors affecting these characteristics were investigated [6]. The leaching rate of the BAC homologues from treated wood in distilled water (DW) was in the order of C12 > C14 > C16. This order of the leaching rates was identical to the order of the homologues with regard to water solubility (C12 > C14 > C16). The leaching rates of the homologues from treated wood were higher in seawater (SW) than in DW and the order of leaching rates in SW was C12 > C14 > C16. Thus, the leaching rate of the homologue having a shorter alkyl chain is higher than that of the homologue having a longer alkyl chain in both DW and SW. This tendency of the C12 homologue to exhibit a higher leaching rate than the C14 homologue was observed in a field experiment in which ACQ-1-treated wood specimens were exposed to marine conditions.

The retention of BAC homologues on wood occurs mainly via cation-exchange mechanisms by the carboxylic and phenolic hydroxyl groups in wood [7, 8]. The BAC homologues retained by these mechanisms can be replaced by inorganic cation species such as Na^+ and Mg^{2+} in SW or H^+ in acidic media. These replaced BAC homologues then undergo leaching easily; thus, SW and acidic media accelerate leaching, and the resulting leaching rates of the homologues depend on their hydrophobicities.

When the specimens were treated with 2 of the 3 homologues (C12, C14, and C16) in combination, the leaching rate of the C14 and C16 homologues from the specimens in SW was lower on treatment with a mixture of these homologues than on treatment with a mixture of C12 and either of these homologues. The leaching rates of the C14 and C16 homologues from the high-retention-level specimens were lower than those from the low-retention-level specimens in SW. The adsorption isotherms plotted for the homologues indicated that lateral hydrophobic interactions among adsorbed BAC homologues became more pronounced as the alkyl chain length increased. The ratio of aggregated BAC to the total BAC adsorbed on the wood increased as the concentration of C14 and C16 in the treatment solution increased. This ratio is considered to be higher for the mixture of C14 and C16 than for other combinations. Thus, it is assumed that the leaching behaviour of the homologues is affected by not only their hydrophbicity but also the formation of BAC aggregates on the treated wood.

Further, the leaching rate of the C12 and C14 homologues in soil (fungus cellar) was higher than that in DW. In general, soil contains inorganic cationic species such as K^+, Na^+, Mg^{2+}, and H^+ that also affect the leaching of BAC homologues in soil. In addition, the leaching rates of the C12 and C14 homologues were higher in leaching medium containing water-extractable wood components than in DW. Thus, it was assumed that the organic matter in the soil also affected the leaching of the homologues.

However, a critical difference was observed between the leaching characteristics in soil and in other

leaching media in that the leaching rate of the C14 homologue from the treated wood was higher than that of the C12 homologue in the former. This result indicates that the leaching characteristics of BAC homologues in soil cannot be reproduced in distilled water, seawater, and acidic water. The leaching rate of the C14 homologue was also higher than that of the C12 homologue when leaching medium containing water-soluble wood components was used, and the rates recorded correlated with the concentration of phenolic compounds in the medium. Furthermore, taxifolin (phenolic compound) induced the higher leaching rate of C14 as compared to C12. Thus, phenolic compounds present in soils or generated during the decay of wood may be responsible for this discrepancy between the results obtained when soil was used and when other media were used.

Based on the results of the present study, the leaching mechanisms of BAC homologues and the effects of environmental factors on these mechanisms have been summarized in Fig. 1. The results indicate that leaching experiments should be conducted to evaluate the performance of wood treated with preservatives containing BAC as the active ingredient under different environmental conditions in which wood is used and with consideration to the various environmental factors it is exposed to. To prevent the leaching of BAC, the appropriate formulation of BAC homologues in wood preservatives should be selected depending on the environments in which the treated wood is used. For wood used in environments exposed to water or SW, BAC that mainly comprises homologues having longer alkyl chains should be used. On the other hand, for wood used in contact with the ground, BAC that mainly comprises homologues having shorter alkyl chains should be used.

For the further improvement of ACO-1-treated wood, future investigations should focus on the effects of combinations of homologues having different alkyl chain lengths on leaching in soil and in media containing phenolic compounds.

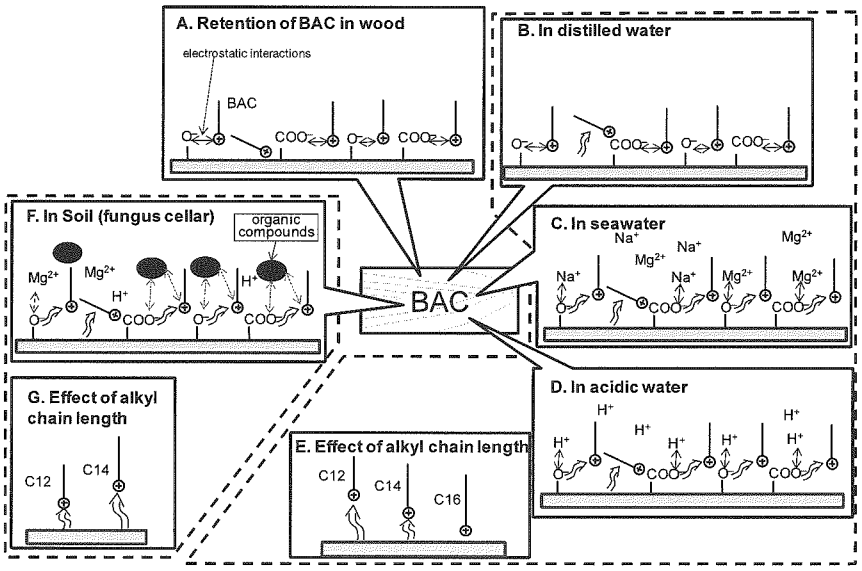

Fig1. Interactions of benzalkonium chloride (BAC) with wood and environmental factors.

[1] Japanese Industrial Standard (JIS) K1570:2004, Japan Industrial Standard Association, Tokyo
[2] Tsunoda K., Ed. Imamura, Y., Press-Net, Kyoto, pp113 (2001)
[3] Miyauchi T., Mori M. and Ito K., Journal of Chromatography A, 2005, 1063, 137–141
[4] Miyauchi T., Mori M. and Ito K., Journal of Chromatography A, 2005, 1095, 74–80
[5] Miyauchi T. and Mori M., Holzforschung, 2007, 61, 337–341
[6] Miyauchi T., Mori M. and Imamura Y., Journal of Wood Science (in press)
[7] Loubinoux B. and Malek H., Holzforschung, 1992, 46, 537–539
[8] Doyle A.K. and Ruddick J.N.R., Holzforschung, 1994, 48, 106–112

Polysaccharide synthesis *in vitro* from cellulose-producing model organisms

Chiori Ito
Laboratory of Biomass Morphogenesis and Information, RISH, Kyoto University

Cellulose is synthesized from terminal complexes (TCs) on the plasma membrane. Globules of TCs are supposed to be cellulose synthase, CesA. However the composition and mechanism of cellulose synthase or TCs are poorly understood. In order to elucidate them, trails to synthesize cellulose *in vitro* were made.

The originality of this experiment lies on the manipulation of membrane-bound cellulose synthase, and its application to *in vitro* synthesis of cellulose. For establishing methods for the *in vitro* synthesis of cellulose, microsomal fraction was collected from different model organisms – tobacco BY2 cells, *Gluconacetobacter*, *Ciona intestinalis*, *Saprolegnia monoïca* and *E. coli* heterogously expressing cellulose synthase of *Gluconacetobacter* (BcsA). In all the cases, cells were disrupted and subjected to differential centrifugation to collect the microsomal fraction. Membrane-bound proteins were further extracted by detergent, for example digitonin, to which UDP-glucose was added to conduct *in vitro* synthesis of cellulose. The product was characterized by electron microscopy, FT-IR and X-ray diffraction, as well as radio isotope assay with UDP-[^{14}C]-glucose. Incorporation of radioactivity to the *in vitro* product was observed for each detergent extract. This confirmed that the analyzed polysaccharides were newly synthesized and not arising from endogenous sources like cell wall.

In the case of BY2, two types of *in vitro* products were observed: fibers and spindles (Figure 1a and 1b). These products were analyzed with ATR-FTIR and X-ray diffraction, and most of them were revealed as (β1→3)-D-glucan. The *in vitro* product from *Ciona intestinalis* was detected only before detergent extraction, and fibers of 5-12 nm in width and indefinite in length were observed (Figure 1c). The *in vitro* product from *Saprolegnia monoïca* was microfibrils, 4-6 nm or some of them are 10-20 nm in width (Figure 1d) as seen in the previous study [1]. The characterization of these products and optimizing parameters for cellulose synthesis *in vitro* are in progress.

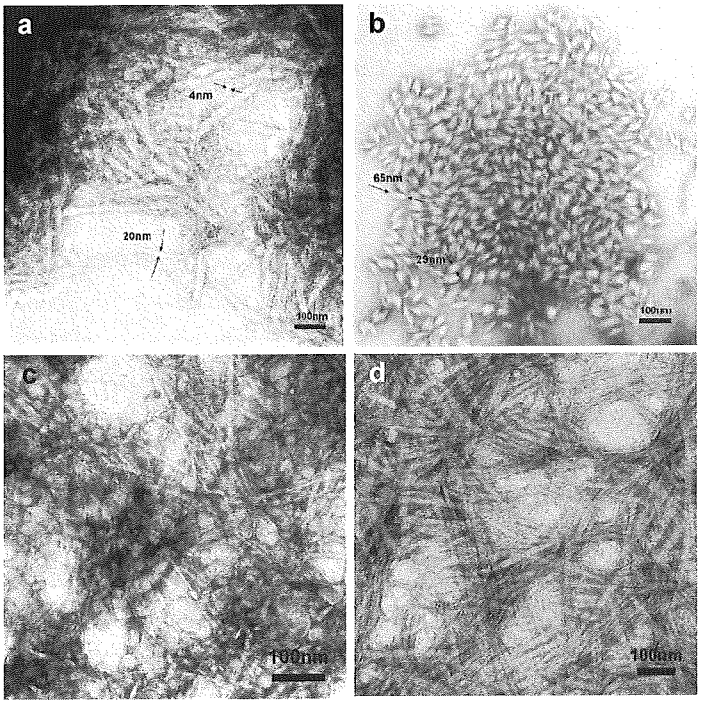

Figure 1
The *in vitro* products from: (a) BY-2 (microfibrils), (b) BY-2 (spindles), (c) *Ciona intestinalis* and (d) *Saprolegnia monoïca*

ACKNOWLEDGEMENTS: I appreciate Prof. Junji Sugiyama and the members of LBMI-RISH for their encouraging throughout this study. This study was partially supported by Grand-in-Aid for Scientific Research (No. 19208017), and conducted in collaboration with Prof. Vincent Bulone (KTH Sweden) and Drs. Keisuke Nakajima and Tomoya Imai (Faculty of Sciences, Kyoto University).

REFERENCE

[1] Pelosi, L. *et al.* (2003) *Biochemistry* **42**, 6264-6274

Transformation vectors utilizing *Ceriporiopsis subvermispora* gene expression signals.

Harunori Kawabe
Laboratory of Biomass Conversion, RISH, Kyoto University

[Introduction]

White rot fungi are known to degrade plant cell wall lignin and also various aromatic pollutants. Recently, wood biomass conversion systems drew attention as one of solutions for environmental problems, since cyclic utilization of wood is carbon-neutral. Delignification is necessary to convert wood biomass effectively, whereas general white rot fungi degrade not only lignin but also cellulose. A selective lignin-degrading fungus, *Ceriporiopsis subvermispora* is able to degrade lignin selectively without intensive damage of cellulose. To elucidate molecular mechanism for the selective lignin degrading system in this fungus, development of an efficient transformation system would make much contribution. This study reports construction of the transformation vectors containing drug-resistant markers driven by gene expression signals isolated from *C. subvermispora* β-tubulin.

[Materials and Methods]

Degenerated primers for amplification of *C. subvermispora* gene fragment encoding for β-tubulin were designed with CODEHOP method. With these primers, A DNA fragment was amplified by PCR and cloned into pGEM-T vector. Then, a whole gene fragment was cloned by using inverse PCR. Plasmids pCsbtubi-*bar* and pCsbtubi-*hph* were constructed by the ligation of *C. subvermispora* β-tubulin promoter and terminator to the bialaphos resistant gene (*bar*) and hygromycin B resistant gene (*hph*), respectively. These vectors contains the first intron of β-tubulin following to the promoter, since Ma *et al.* reported the presence of a 5' intron accerated the expression of recombinant *egfp* gene in *P. chrysosporium*[1].

To estimate these vectors function in *C. subvermispora*, they were introduced to *P. ostreatus* mediated PEG/$CaCl_2$. Genome DNAs were extracted from resultant drug-resistant isolates and subjected to PCR analysis and Southern blotting. In Southern blotting, DNAs were digested with *Hin*d III and *Xba* I and transferred to the nylon membranes (Roche).

[Results and Discussion]

PCR analyses of DNA of the drug-resistant isolates obtained from transformation experiments with pCsbtubi-*bar* and pCsbtubi-*hph* demonstrated specific amplification of the marker fragment in most cases. Drug-resistant isolates without specific amplication of the fragment were suggested to be backgrounds or transient transformants. After five successive cultivation in the absence of drug selection, 7 bialaphos-resistant transformants were subjected to Southern hybridization. Several hybridizing bands were detected in the transformants with stable drug-resistance, whereas no hybridizing signals were observed in the those with transient drug-resistance as well as wild type control. These results confirmed that the introduced *bar* gene functions in these stable transformants. Southern hybridization analysis for hygromycin-resistant isolates, several bands of different sizes were detected in the transformants, suggesting that the probe might be not appropriate and further detailed analysis is required. These results suggested that pCsbtubi-*bar* and pCsbtubi-*hph* functioned in basidiomycete and hereby these vectors will work properly in *C. subvermispora,* from which the gene expression signals were isolated homologously.

[Reference]

1) Ma B., Mayfield M.B., and Gold M.H. (2001) *Appl. Environ. Microbiol.* **67**: 948-955

Studies on selective white rot by *Ceriporiopsis subvermispora*

Takahiro Hasegawa
Laboratory of Biomass conversion, RISH, Kyoto University

A selective lignin-degrading fungus, *Ceriporiopsis subvermispora*, can degrade lignin without intensive damage of cellulose. We have demonstrated that extracellular lipid peroxidation by manganese-dependent peroxidase (MnP) occurred in the selective white rot by *C. subvermispora*. At an incipient stage of wood decay, this fungus produced MnP and large amounts of unsaturated and saturated long chain fatty acids, leading the generation of radicals [1]. Moreover, ceriporic acid B (1-nonadecene-2,3-dicarboxylic acid), an extracellular metabolite produced by *C. subvermispora,* inhibits the generation of cellulolytic and ligninolytic hydroxyl radicals [2]. These observations suggest that extracellular enzymes and low molecular mass metabolites play key roles in the selective lignin degradation. However, the selectivity by *C. subvermispora* changes in various culture conditions [3-4]; thereby it has remained to be elucidated what factors are required for the selective lignin degradation.

In the present study, we investigated degradation patterns of wood cell wall components, activity of ligninolytic enzymes, and production of metabolites, such as fatty acids and ceriporic acids by *C. subvermispora* under various conditions. On wood meal cultures, the selectivity of lignin degradation under low nitrogen condition was much higher than in high nitrogen media. The significant lignin loss was found when both high MnP activity and decrease in accumulated linoleic acid were concomitantly observed, suggesting that lipid peroxidation is involved in the ligninolysis. On a synthetic liquid medium, furthermore, the concentration of nitrogen significantly affected the lipid metabolic profiles. Large amounts of linoleic acid were secreted by the fungus by addition of lignin fragments under high nitrogen conditions. These observations shed light on candidate factors involved in the selective lignin degradation by *C. subvermispora*.

REFERENCES

[1] Enoki, M., Watanabe, T., Nakagame, S., Koller, K., Messner, K., Honda, Y. and Kuwahara, M. (1999) *FEMS Microbiol. Lett.*, **180**: 205-211.
[2] Watanabe, T., Teranishi, H., Honda, Y. and Kuwahara, M. (2002) *Biochem. Biophys. Res. Commun.*, **297**: 918-923.
[3] Otjen, L., Blanchette, R., Effland, M. and Leatham, G. (1987) *Holzforschung*, **41**: 343-349.
[4] Blanchette, R., Burnes, T., Eerdmans, M. and Akhtar, M. (1992) *Holzforschung*, **46**: 109-115.

MOLECULAR CLONING AND CHARACTERIZATION OF *CAD* AND *OMT* GENES INVOLVED IN LIGNIN AND LIGNAN BIOSYNTHESIS

Safendrri Komara Ragamustari

Laboratory of Metabolic Science of Forest Plants and Microorganisms, RISH, Kyoto University

Lignin and lignans are typical phenylpropanoid compounds derived from the cinnamate/monolignol pathway. Lignins confer mechanical strength to plant cell walls and the plant as a whole, while lignans have a wide variety of biological functions and activities, not only for the plant itself, but also for other organisms.

In the author's current research, the author has tried to elucidate genes that are involved in lignin and lignan biosynthesis. To do so, the author has conducted experiments to isolate cDNAs which are possibly involved in lignin/lignan biosynthesis, and characterize their recombinant proteins.

Characterization of *Carthamus tinctorius* cinnamyl alcohol dehydrogenases

Cinnamyl alcohol dehydrogenase (CAD) is an NADPH-dependent enzyme that is known to be responsible for the last reductive step in the monolignol biosynthesis, where coniferaldehyde and sinapaldehyde, are reduced into their corresponding monolignols, coniferyl alcohol and sinapyl alcohol. This is thought to be one of the factors in determining the lignin content in wood. In the current research, the author carried out the characterization of three cDNAs encoding cinnamyl alohol dehydrogenase (CAD) in *Carthamus tinctorius* (safflower), which were named *CtCAD1*, *CtCAD2*, and *CtCAD3*, respectively. The plant was chosen due to its significant amount of lignin and lignan production in its seed developing stage.

In this research, the author conducted functional characterization of the recombinant CtCADs by use of GCMS-based analysis. In addition, the author also carried out quantification of *CtCAD* expression in different *C. tinctorius* tissues.

Molecular cloning of *Anthriscus sylvestris O*-methyltransferase cDNAs

S-Adenosyl-L-methionine (SAM)-dependent *O*-methyltransferases (OMTs) play important roles in plant secondary metabolite biosynthesis. They are involved in the synthesis of methylated plant phenolics, including lignin, lignan, flavonoids, and other phenylpropanoids. These plant OMTs transfer a methyl group from SAM to the hydroxyl group of the methyl acceptor.

In order to further understand the roles of *O*-methyltransferases (OMTs) in the biosynthesis of an antitumor lignan, podophyllotoxin, via yatein, the author isolated seven *OMT* cDNAs from an *Anthriscus sylvestris* (cow parsley) cDNA library. *A. sylvestris* was chosen because it produces significant amount of yatein. Substrates of the recombinant OMTs will be determined by GCMS-based assay analysis.

Gene discovery of the regulatory factors for wood formation by gene co-expression network analysis

Yoshinori Takahashi

Laboratory of Metabolic Science of Forest Plants and Microorganisms

Wood is mainly composed of cellulose, hemicellulose and lignin. Lignin is a phenolic polymer mainly derived from three monoligninols — coniferyl, sinapyl and 4-coumaryl alcohols. Monolignols are synthesized via the cinnamate/monolignol pathway (CMP), and finally polymerized by peroxidases. While many genes encoding CMP enzymes have been characterized until now, the regulatory mechanism of the gene expression by transcription factors is not well-known. To identify the function of the transcription factors involved in lignin biosynthesis, the gene co-expression network analysis by using microarray datasets of *Arabidopsis thaliana* is one of the prospective methods.

In this study, the author performed the gene co-expression network analysis with *A. thaliana* microarray datasets and narrowed down the candidate genes. Three candidate genes, which showed the expression pattern correlated with several CMP genes, *AtRING1*, *AtRING2* and *AtNAC1* were further characterized.

The author profiled the expression pattern of the genes involved in secondary cell-wall synthesis in each inflorescent stems of T-DNA insertion lines for *AtRING1*, *AtRING2* and *AtNAC1*. As a result, significant difference in the expression of the genes involved in cell-wall synthesis including CMP genes and *CesA* was found between T-DNA insertion and wild type lines.

We next measured the lignin content of T87 cells over-expressing *AtRING1* by acetyl bromide method. The lignin content was the same as the control. On the other hand, microarray analysis of T87 cells over-expressing *AtRING1* indicated that peroxidases were over-expressed in the cells. The above results suggested that up-regulation of *AtRING1* did not result in the change of lignin content, but resulted in the change of gene expression involved in cell-wall formation.

Galactinol Synthase Gene of *Coptis japonica* is Involved in Berberine Tolerance

Kojiro Takanashi
Laboratory of Plant Gene Expression, RISH, Kyoto University

Many plant secondary metabolites show strong biological activities and potentially also toxic to plants, while plants producing those active compounds are usually insensitive to their own metabolites, suggesting that they have a species-specific detoxification mechanism. In order to clarify the detoxification mechanism of alkaloid, we used cultured cells of *Coptis japonica*, which are capable of producing a yellow isoquinoline alkaloid berberine and accumulate it in the vacuole, and show strong tolerance for berberine, unlikely to other plant cells that do not produce berberine. We established a fission yeast strain that was sensitive to berberine, with which a functional screening using *C. japonica* cDNA library was performed. One cDNA clone, which conferred clear berberine tolerance, encoded galactinol synthase (CjGolS).

GolS is known to catalyze the first committed biosynthetic step for raffinose family oligosaccharides (RFO). GolS utilizes UDP-galactose and *myo*-inositol as substrates to form galactinol, and this enzymatic reaction step reportedly plays a key regulatory role in the carbon flux branching between sucrose and RFO. To determine the reason for the berberine tolerance conferred by CjGolS, the berberine content in CjGolS-expressing yeast cells was measured by HPLC. The cellular levels of berberine in CjGolS-expressing yeast grown in 25 μM or 50 μM berberine-containing medium were not significantly different from the berberine levels in the control cells.

The expression levels of *CjGolS* in various organs of intact plant and cultured cell lines of *C. japonica* were analyzed by semi-quantitative RT-PCR analysis. The *CjGolS* gene was expressed in all parts of the plant, preferentially in the aerial parts, petioles, and leaves (Fig. 5A), where berberine was not produced or highly accumulated. Whereas, the steady-state level of *CjGolS* expression was higher in 156-S, which produces about 3-fold higher amounts of berberine as compared to CjY, a low berberine-producing line (Fig. 5B).

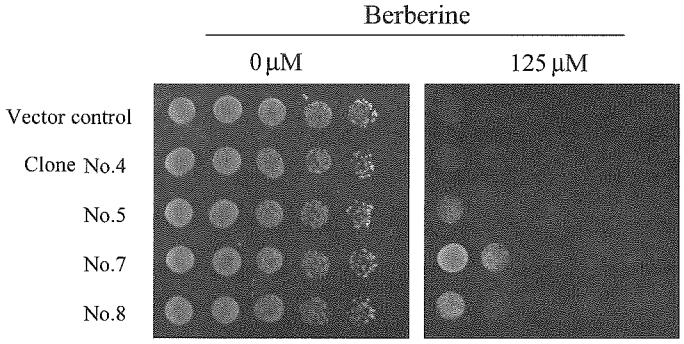

Fig. 1. Screening for Berberine-Tolerance Genes in *C. japonica* cDNA Library.

These panels show the 3rd screening round, in which the plasmid containing the berberine tolerance cDNA identified in the 1st and 2nd screening rounds was reintroduced into fission yeast as the 3rd screening round. Clone No.7, which encoded galactinol synthase (CjGolS), showed distinct berberine tolerance.

Utilization of Bowman-Birk proteinase inhibitor for prevention of cadmium influx to plant cells.

Ayako Majima

Laboratory of Plant Gene Expression, RISH, Kyoto University

Cadmium is a toxic heavy metal that causes serious environmental pollution in many countries. Especially, cadmium pollution is serious in Japan due to the large consumption of this heavy metal for the production of batteries and other products. The most serious cadmium pollution is seen in rice, the major food for Japanese nations. In order to establish plants that do not absorb cadmium in the body, we were screening *Coptis japonica* cDNA library for cadmium tolerant genes by use of yeast as the host organism. Among cadmium tolerant clones have found that a Bowman-Birk proteinase inhibitor gene (Fig. 1), which gave stronger tolerance to cadmium than metalothionein, a well-known heavy metal tolerant protein (Fig 2).

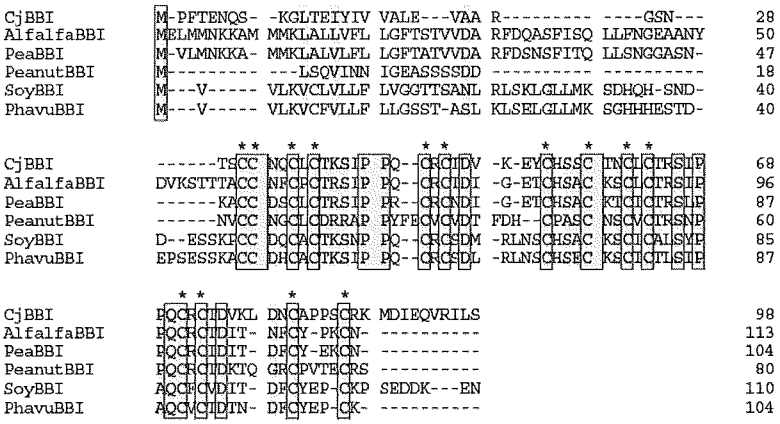

Figure 1. Multiple alignment of Bowman-Birk proteinase inhibitors

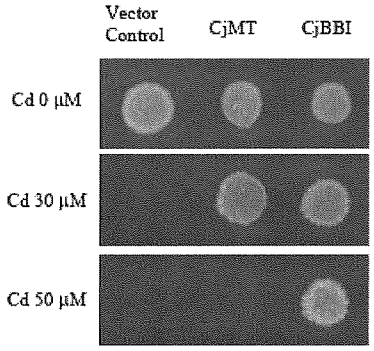

Figure 2. Cadmium tolerance of yeast transformatns.
MT, metalothionein

Regulatory mechanism of product specificity of FPP synthase providing GPP as the specific product in *Lithospermum erythrorhizon*

Tatsuya Miyawaki

Laboratory of Plant Gene Expression, RISH, Kyoto University

Terpenoids occur in all organisms characterized so far. In particular, plants produce a large variety of terpenoid compounds, which are classified into hemi-, mono-, sesqui-, di-, tri- and tetraterpenoids according to the number of carbons in the molecules that correspond C5, C10, C15, C20, C30 and C40 (carotenoid) compounds. Among them, monoterpenoids consist of major flavor components in plants. These C10 compounds are biosynthesized in plastids from geranyl diphosphate (GPP) provided in vivo by GPP synthase (GPPS), whereas there is only one exception of cytosol-localized GPPS that is reported in Lithospermum erythrorhizon, a boraginaceous plant. In order to clarify what kind of polypeptide is responsible for the production of GPP in cytosol and what is the regulatory mechanism of the chain elongation, we systematically cloned putative prenyl diphosphate synthases from the EST library of *L. erythrorhizon*.

Figure shows the subcellular localization of known prenyl diphosphate synthases, either in plastid or in cytosol. There are two types of GPP synthases, one is that functioning as a homodimer and the other is active as a heterodimer (shown in pink), while FPP synthase is cytosol-localized and functioning as a homodimer. The cytosol GPPS of *L. erythrorhizon* is presumed to be either a mutated FPPS having product specificity for GPP or a hetoromer FPPS with an unknown regulatory subunit. Both possibilities have been examined with cell-free extract of cultured *L. erythrorhizon* cells.

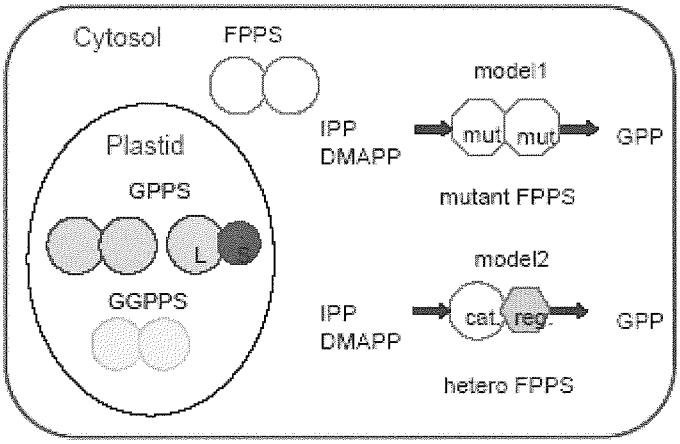

Figure. Two hypothesis of cytosol-localized GPPS

MATE-type transporters responsible for the vacuolar accumulation of alkaloid in tobacco.

Masahiko Morita

Laboratory of Plant Gene Expression, RISH, Kyoto University

Higher plants produce a large number of secondary metabolites, such as alkaloids, terpenoids, and phenolic compounds. They are often accumulated in particular sink organs, and some are translocated from source cells via long distance transport. The membrane transport of plant secondary metabolites is a newly developing research area. Recent progress in genome sequencing projects.

One of the most well-known examples of long-distance transport is nicotine alkaloids in *Nicotiana* species. Nicotine is biosynthesized in root tissues, where it is specifically increased in the response to attacks by pathogens and herbivores, and the produced nicotine is translocated to the aerial part for accumulation (Figure). As a model system we have been using tobacco plants, and studying the transporter molecules responsible for the membrane transport of nicotine and related alkaloids.

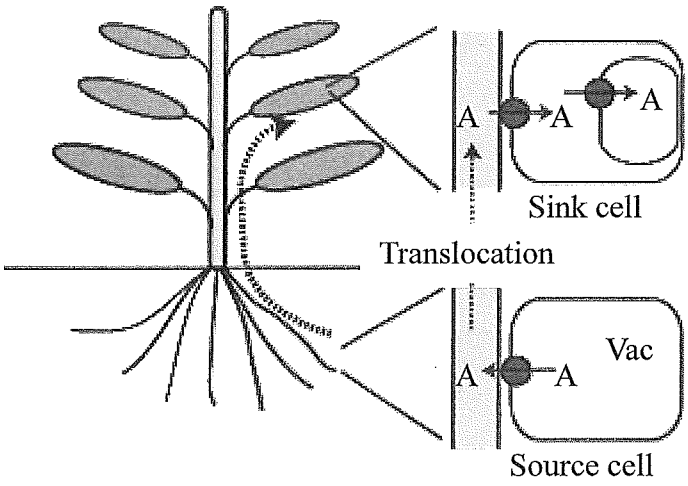

A, alkaloid; V, vacuole; X, xylem

Figure. Scheme of long-distance transport of alkaloids in plants

F Development of an algorithm to derive gridded dataset from GPS occultation data

Yosuke Azuma

Laboratory of Atmospheric Sensing and Diagnosis, RISH, Kyoto University

The Global Positioning System (GPS) radio occultation (RO) observations, where signals from the GPS satellites are received by low-earth-orbit satellites to measure vertical profiles of atmospheric parameters such as temperature and humidity was started in mid 1990s. It is a calibration-free method with a high vertical resolution. Until recently, GPS RO measurements were done mostly with one or two satellites at a time. Thus, its data density was not high, and the majority of past studies were based on analyses of vertical profiles. However, in April, 2006, data from the COSMIC/FORMOSAT-3 mission, which consists of six low-earth-orbit (LEO) satellites, were launched, so the data density was dramatically increased. Therefore, it is now easier to study spatial structures of atmospheric phenomena. Until one year after the launch, multiple COSMIC satellites were in a same orbit, so the data density was especially high in its vicinity. This study proposes a method to make gridded datasets by exploiting this feature.

A coordinate system based on the swath around the orbit was introduced, and an iterative algorithm to conduct the coordinate transformation of occultation data points was proposed. Gridded datasets were made by linearly interpolating among a mesh derived by the Delaunay triangulation. From the results, features of the distribution of the RO data points and its impact on the gridding were discussed. Case studies were made on the tropical tropopause layer and the northern high-latitude stratosphere. It is shown that the three-dimensional structures of mesoscale waves were captured in the gridded data. Errors due to the interpolation were estimated by using objective analysis data. If the interpolation was restricted to occur over distances less than 2000 km, the error was comparable to the error in the objective analysis itself. In this case, the ratio where valid data were obtained in the swath with a 4000-km width was a little higher than 20 %. Even in that case, the case studies showed the usefulness of the data. If more satellites were used in future missions, the method proposed in this study will be further useful by providing more complete swath data.

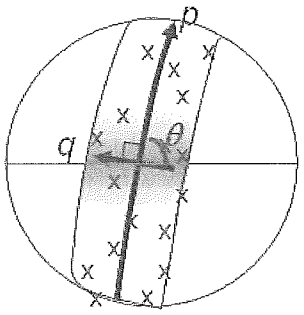

Figure 1: Schematic illustration of the coordinate along the orbits of COSMIC LEO satellites. The p coordinate follows the trajectory of the satellites, and it is closely related to time.

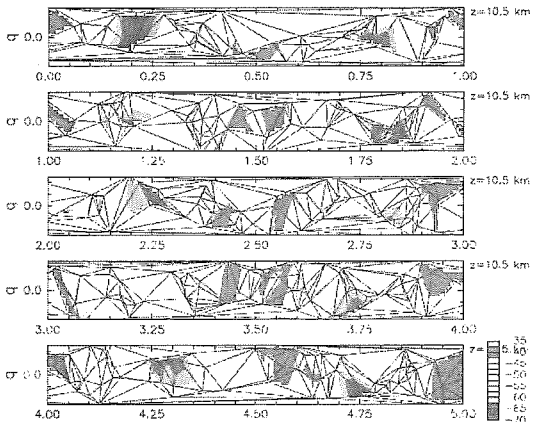

Figure 2: The Delaunay triangles and the gridded temperature at the altitude of 10.5 km obtained from the occultation data in the first 5 satellite circles in Dec 1, 2006. Here, data from 4 satellites in one orbit were used.

Observation of water vapor distribution in the lower troposphere in the sub-tropical region of Okinawa by a portable Raman lidar

Yosuke Sato

Laboratory of atmospheric sensing and diagnosis, RISH, Kyoto University

Water vapor effects on various atmospheric phenomena significantly through transportation of latent heat, cloud formation, precipitation etc.. Therefore, it is important to observe spatial and temporal variation of water vapor with a high time and spatial resolution in order to reveal its characteristics. A Raman lidar is an active remote sensing technique of profiling atmospheric parameters, including water vapor mixing ratio. We have developed portable Raman lidars for profiling water vapor at various observation sites. In this study, we have build up a stable automatic and remote observation system of small Raman lidar to be used in Okinawa, the sub-tropical region. The observation in Okinawa was initiated in April 2006, and profiles of water vapor mixing ratio and back scatter ratio up to about 3–4 km have been continuously observed with 0.5–1 hour resolution and 60–480 m height resolution, dependent on altitude (Figure 1). The observed data are automatically processed and stored in the database, which is open through web page. Comparison of the lidar observation with routine radiosonde observation at Naha, Okinawa showed that the spatial variety of water vapor at about 70 km horizontal distance was correlated with the temporal variability during the night by lidar observation especially around winter (September to March), when advection of water vapor due to synoptic scale motion. We further compared water vapor profile observed by the lidar with those derived from GPS occultation measurement, COSMIC. We have compared 11 profiles within 100 km distance, and found that observed difference of water vapor between the two technique at 1.0–2.3 km altitude did not show significant bias, when compared with the spatial difference estimated by the lidar observation. We also stress that in order to observe local distribution of water vapor which cannot be obtained by satellite, stable and automatic ground based observation such as Raman lidar is a useful technique.

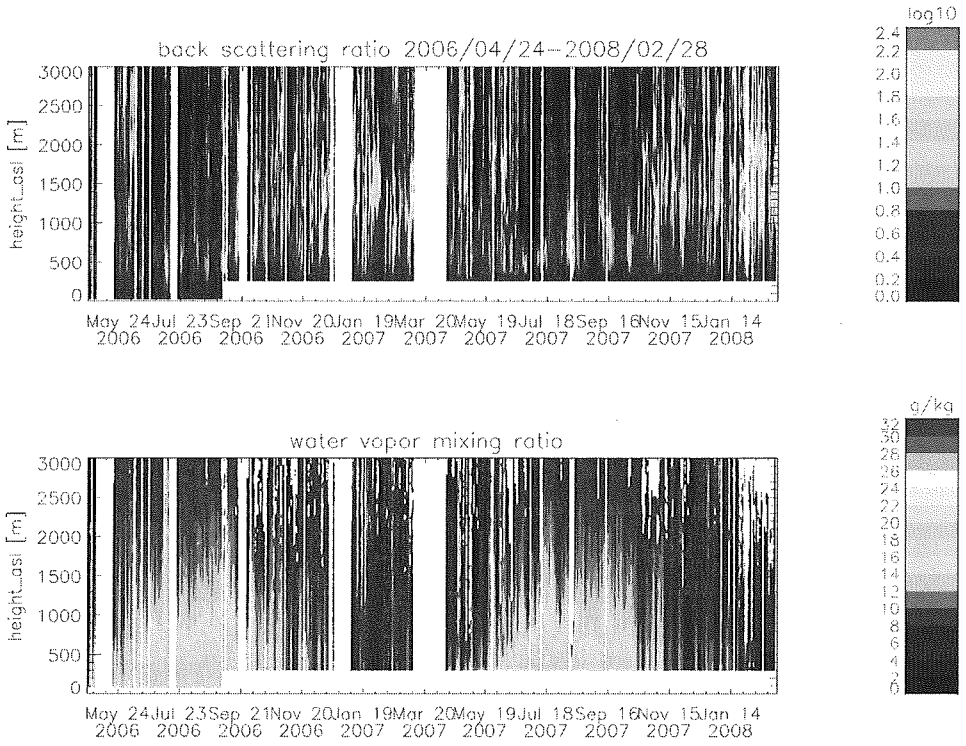

Figure 1. Backscatter ratio (clouds/aerosol content) (top) and water vapor mixing ratio (bottom) observed in Okinawa between April 24, 2006 and February 28, 2008. Nightly average is plotted. Observation sites before and after September 2, 2006 were Onna(26.5N, 127.8E, 8m ASL), and Ogimi(26.7N, 128.1E, 225m ASL), respectively.

Study of coupling processes between mid-latitude ionospheric E and F regions based on the FERIX-2 experiment

AOKI Yuichi
Laboratory of Radar Atmospheric Science, RISH, Kyoto University

In the ionosphere, conductivity parallel to the geomagnetic field is so high that such polarization electric fields are easily mapped along the field line for several hundred kilometers. Therefore, it had been expected that FAIs in the E- and F- regions are geomagnetically coupled.

FERIX (F- and E- Region Ionosphere Coupling Study) observation campaign was carried out in 2004. We located LTPR (Lower Thermosphere Profiler Radar) at Sakata to observe E-region FAI, and with the MU radar, observed F-region FAI from Shigaraki. By the observations, E- and F- region FAIs were found at the same time along the same geomagnetic field lines. However, important problem was left unsolved, i.e., which region contributes to the generation of the electric fields. We then conducted the similar experiment FERIX-2 from May to September 2007. For FERIX-2 experiment, we applied the radar imaging technique for both radars, and studied the horizontal structures of both E- and F- regions FAIs in more detail. We also operated a bistatic receiving site at Maze, Niigata to expand observation region of the LTPR. Observations of Doppler velocity of the echoes from both Sakata and Maze would reveal two dimensional motion of the E-FAI.

From these observations, we found that the F-FAI shows northwest-southeast wavefont with small structures of 20-30 km. The small structures had wavefront various Doppler speed, and propagated to the northwest. On the other hand, E-FAI distributed zonally elongated, or showed northwest-southeast structures. Although the difference of the scale was pointed out in E-layer and F-layer, close structure between E-FAI and F-FAI was discovered. We found that E-FAI were enhanced and showed northwest-southwest wavefront structures when F-FAI echoes were observed by the MU radar. The overall horizontal motions of the F-FAI and E-FAI echoes are simillar and westward, as originally reported from FERIX-1. The radar imaging observations, however, revealed that smaller echo patches of E-FAI tend to appear at the edge or around the F-FAI echoes.

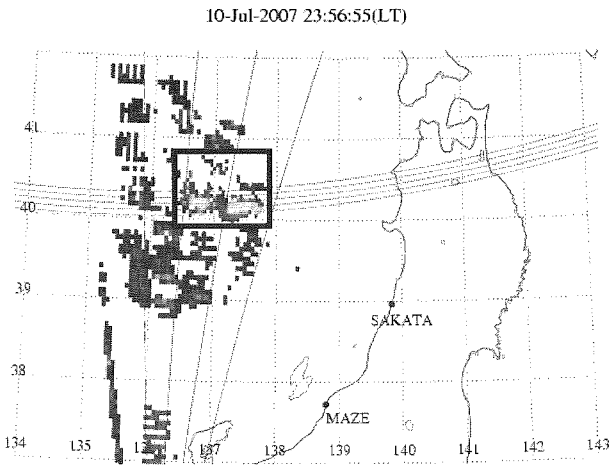

Figure: Horizontal distribution of F-region FAI echoes observed with the MU radar. The echoes are obtained by the MU radar multibeam imaging observations. The F-region FAI echoes are found at 250-300 km altitudes, but in this figure, they are mapped down to 100 km altitude along the geomagnetic field line. Shown in the square area is the E-region FAI echo distribution observed by the LTPR located in Sakata. Close comparison between F- and E-region observations revealed that E-region FAI echoes tend to appear at the edge of the F-region FAI echoes.

Observation of vertical air motion in midlevel shallow-layer clouds by the Equatorial Atmosphere Radar and lidar

KISHI Toyohisa
Laboratory of Radar Atmospheric Science, RISH, Kyoto University

Shallow-layer clouds are confined to shallow layers of air in which the rate of cooling resulting in cloud formation is rather slight. These clouds are generally about 1 km or less in vertical extent, and include low-level ones (fog, stratus, and stratocumulus), midlevel ones (altostratus and altocumulus), and high-level ones (cirrus, cirrostratus, and cirrocumulus). Though shallow-layer clouds can occur quite locally, they can also be very widespread, covering mesoscale or even synoptic-scale regions. This prosperity of shallow-layer clouds to cover great areas has a major impact on the climate of the earth through the absorptive and scattering effects of these cloud layers in the earth's radiation balance. Though mean vertical air motion in shallow-layer clouds is smaller compared with ones in convective clouds, previous numerical computations have shown that vertical air velocity (hereafter W) plays a crucial role in the formation and maintenance of shallow-layer clouds. However, observations of W in and around shallow-layer clouds are scarce because means to measure W are limited.

VHF Doppler radars observe height profiles of vertical and horizontal winds by receiving echoes from fluctuations of refractive index and hence have the capability to directly observe them both in clear and cloudy regions. Lidars which lase for transmission are useful for observing vertical profiles of small-sized cloud particles with a diameter of less than several hundred micrometers, due to their short wavelength transmitted. In this study, VHF (47-MHz) Doppler radars named as the Equatorial Atmosphere Radar (hereafter EAR) and 532-nm lidar operated by Tokyo Metropolitan University were used to observe W in and around midlevel shallow-layer clouds with high time and vertical resolutions (167 sec and 150 m, respectively). Frequency power spectrum data obtained with vertically-pointed radar beam were used to obtain W and and spectral width. Spectral width is a measure of turbulent intensity of W within sampling time and volume.

Figure shows a time-altitude plot of spectral width observed by the vertically-pointed radar beam of the EAR. Within the clouds, turbulent motion (spectral width of greater than 0.4 m s^{-1}) was observed in the upper part of shallow layer clouds. In the upper part of clouds (around 8.215 km), downward W was dominant. In the middle part (around 7.615 km), highly turbulent W was observed. In the bottom part (around 6.415 km), turbulence of W was small (figures not shown). Such features found in W were observed for the first time.

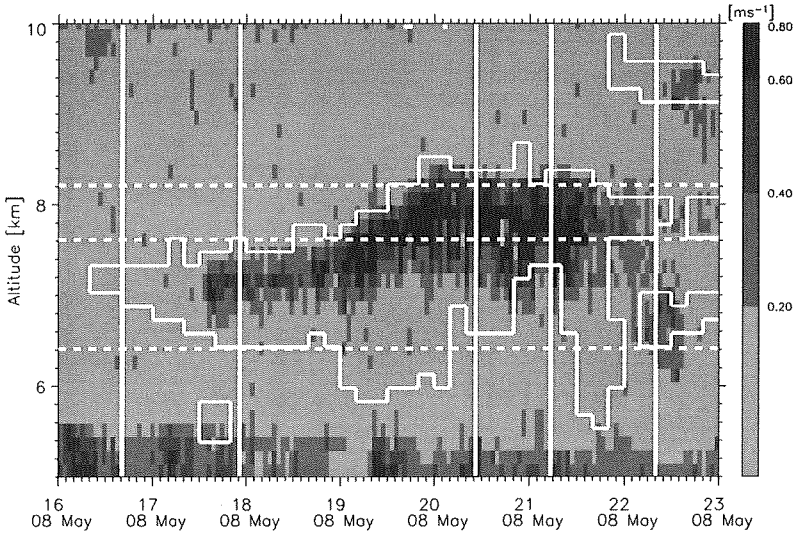

Figure: Time-altitude plot of spectral width observed by the vertically-pointed radar beam of the EAR from 1600 to 2300 LST 8 May 2004. Spectral width is defined as half-power full-width. Thick white curve indicates cloudy area where lidar observed significant enhancements of received signal. Three white broken lines show altitude near cloud top (8.215 km), middle of clouds (7.615 km), and cloud bottom (6.415 km).

Wind Profiler Radar Observations over Indonesian Maritime Continent

TABATA Yoshikazu
Laboratory of Radar Atmospheric Science, RISH, Kyoto University

The Indonesian Maritime Continent (IMC) consists of about 17500 islands surrounded by seas with the warmest surface temperature in the world. Because of wealthy water vapor supply from warm seas and heating by strong solar radiation, it is one of the most active convection regions on the globe. Diurnal variation is the most prominent meteorological phenomenon over IMC. In the active phase of Intraseasonal variation (ISV), Super Cloud Cluster (SCC) passes through IMC, and is thought be modulated by topography of IMC. However, in the eastward region from Sumatera Island, the lack of observational data have prevented from studying such meteorological features.

Under the project of HARIMAU (Hydrometeorological Array for ISV-Monsoon Automonitoring), two wind profiler radars (WPRs) were installed at Pontianak (West Kalimantan) and Biak (Papua) in February and March 2007, respectively (see Figure). Local characteristics of convective activity around two areas are investigated.

By the following results, it was found that Biak had a feature of offshore region over New Guinea Island, while Pontianak had a feature of land.

- Diurnal variation of horizontal wind at Pontianak is consistent with sea-land breeze of Kalimantan Island, whereas that at Biak is consistent with sea-land breeze of New Guinea Island.
- Development of the mixing layer is clearly seen at Pontianak, but is not so clear at Biak.
- Maximum precipitation occurrence is 15 LT at Pontianak, and deep convective clouds are dominant around that time. During 18-2 LT, stratiform type clouds are dominant.
- Maximum precipitation occurrence is 5-12 LT at Biak, and stratiform clouds are dominant in that period.

In Kalimantan Island, cumulus activity starts around the coastline and migrates to inland, which is different from earlier study in Sumatera Island. On the other hand, cloud system migrates offshore direction around New Guinea Island.

During the passage of SCC in the active phase of ISV, diurnal cumulus activity exists, but less dominant at Pontianak. Precipitations did not concentrate on SCC passage period. On the other hand, diurnal cumulus activity was not seen and precipitation concentrated on SCC passage at Biak. Dry air intrusion was seen at Pontianak, but not seen at Biak. Further investigation of SCC is needed for further understanding of intraseasonal variations.

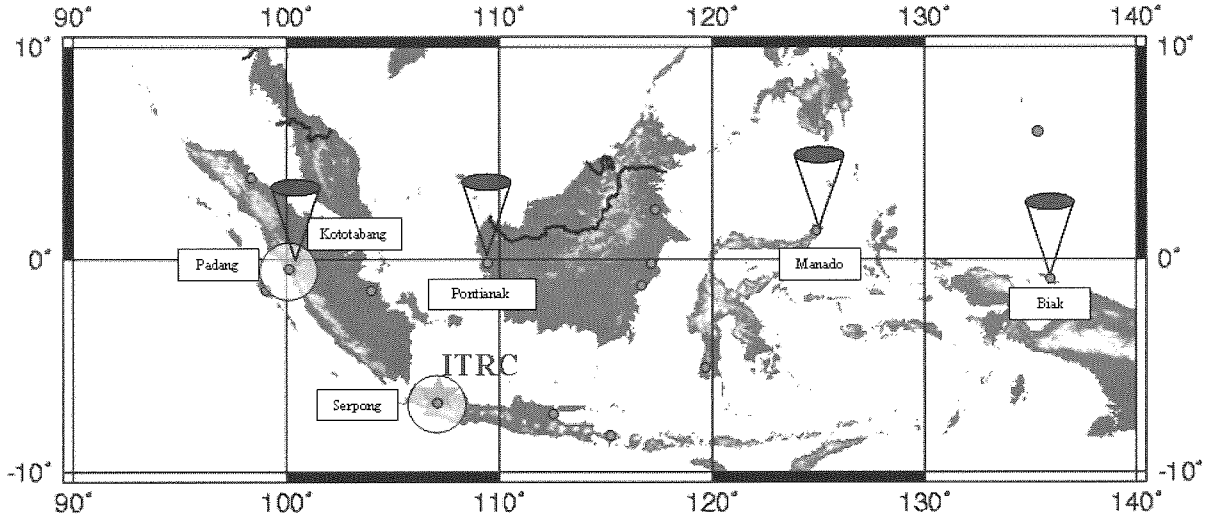

Figure: Distribution of radars and profilers planned by HARIMAU in addition to preinstalled Japanese equipment. ITRC shows International Tropical Research Center Planned to be established in Jakarta. Another WPR is going to be installed at Manado in 2008.

Thermal and Mechanical Properties of Cellulose Nanofiber Reinforced Semi-Crystalline PLA

Lisman Suryanegara

Laboratory of Active Bio-based Materials, RISH, Kyoto University

INTRODUCTION

Polylactic acid (PLA) is a versatile polymer made from renewable agricultural raw materials, which are fermented to produce lactic acid. PLA can be processed similarly to polyolefins or other thermoplastics. The main drawback of PLA for industrial application is the time required to crystallize resulting in longer injection molding cycles compared to, e.g. polypropylene. The present study consisted of evaluating the thermal and mechanical properties of cellulose nanofiber reinforced semi-crystalline PLA in order to assess the possibility to reduce the molding cycle time by accelerating crystallization while improving the thermal and mechanical properties.

MATERIALS AND METHODS

MFC was dispersed in PLA dissolved in dichloromethane. The mixture was dried at room temperature followed by vacuum-drying and a kneader was used to obtain a homogeneous compound. The compound was hot pressed into sheets and cooled by liquid N_2 to obtain completely amorphous samples. Some of them were subjected to annealing to obtain samples with different degrees of crystallinity. The thermal and mechanical properties were evaluated by dynamic mechanical analysis (DMA). The crystallization behavior of PLA was investigated by differential scanning calorimetry (DSC).

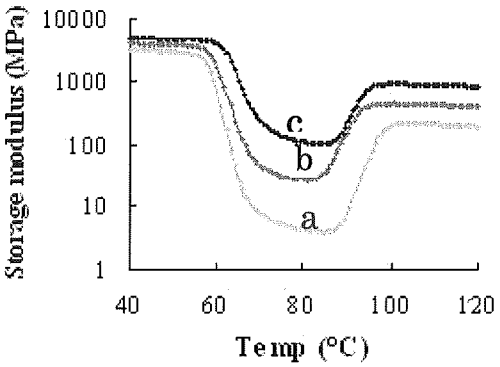

Fig. 1 Temperature dependence of storage modulus of: a) neat PLA, b) 5wt% MFC/PLA, and c) 20wt%MFC/PLA composites

RESULTS AND DISCUSSION

Fig. 1 shows the temperature dependence of storage modulus of neat PLA and MFC/PLA composites. At glassy state, the storage modulus is almost the same for all samples until the softening temperature. The addition of MFC at a fiber content of 20wt% increased the softening temperature of neat PLA from 58°C to 62°C and improved the storage modulus by 27 times at 80°C (rubbery state). The similar result reported in a previous study[1].

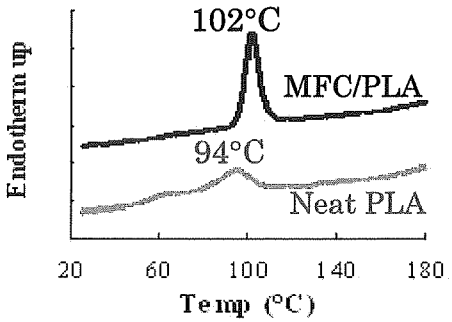

Fig. 2 DSC thermograms of neat PLA and 5wt%MFC/PLA on cooling cycle.

Fig. 2 shows the DSC thermograms of PLA and MFC/PLA composite. During the cooling cycle, the melt crystallization peak of MFC/PLA composite is higher and occurs earlier than neat PLA, indicating that the presence of MFC accelerates the crystallization.

These experiments showed that the reinforcement effect of MFC in PLA composite is effective to improve the thermal and mechanical properties. Moreover, the presence of MFC can act as nucleating agent in PLA crystallization and is expected to reduce the cycle time in injection molding of PLA.

REFERENCE

1) Iwatake A, Nogi M, Yano H. Cellulose nanofiber reinforced polylactic acid. *Comp Sci Tech* 2008. In press

Interfacial control of cellulose nanofiber / thermoplastic resin composite

Kentaro Takagi
Laboratory of Active Bio-based Materials, RISH, Kyoto University

INTRODUCTION

Microfibrillated cellulose (MFC), which is mechanically nano-fibrillated pulp into nanofibers forming a web-like network, shows much promise as reinforcement for plastic. However, the inherent incompatibility between cellulose fibers and hydrophobic thermoplastic resin usually yields poor interfacial adhesion. This study focuses on the improvement of the interfacial adhesion between MFC and the resin (poly (lactic acid): PLA and polypropylene: PP) by esterification of MFC and/or addition of maleic anhydride grafted resins.

MATERIALS and METHODS

MFC (DAICEL CHEMICAL INDUSTRIES, LTD.) was modified by acetylation, butylation or stearylation. The water in modified MFC or untreated MFC slurry was replaced by solvent (acetone for PLA and xylene for PP), and 1wt% MFC in solvent suspension was prepared. When the MFC was thoroughly dispersed in the solvent by stirring, PLA or PP was gradually added. The mixture was dried at room temperature followed by vacuum-drying and a kneader was used to obtain a homogeneous compound. The compound was hot-pressed into films. Maleic anhydride grafted PLA (MA-PLA) and PP (MA-PP) was added to the composites reinforced with untreated MFC and acetylated MFC, respectively.

RESULTS and DISCUSSION

Fig.1 shows the stress-strain curves of tensile test of esterificated MFC5% / PLA composites. Mechanical properties of the acetylated, propionylated and butylated MFC5% / PLA composites are higher than that of untreated MFC / PLA composite. FE-SEM micrographs of fractured surface for composites samples evidenced to improve the interfacial adhesion.

However, mechanical properties of PLA reinforced with stearylated MFC was decreased and FE-SEM micrographs of fractured surface for this composite confirmed the deterioration of the interfacial adhesion

Fig.2 shows the stress-strain curves of tensile test of MFC5% / PP composites to added in MA-PP as a compatibilizer. the addition of MA-PP improved the mechanical properties of all amoposites. FE-SEM micrographs of fractured surface for composites observed the improvement of the interfacial adhesion.

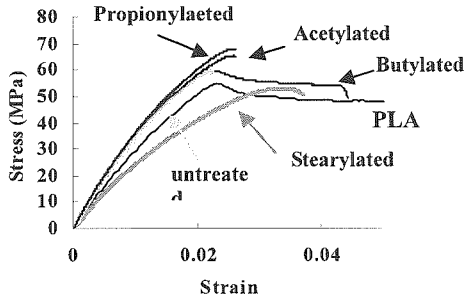

Fig.1 Stress-strain curves for composites reinforced with 5wt% acetylated, propionylated, butylated, and stearylated MFC

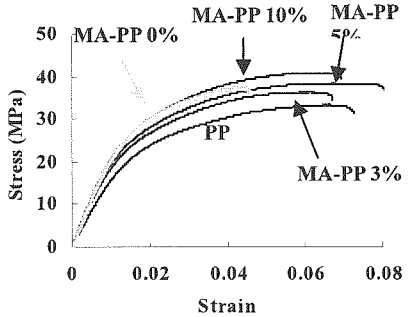

Fig.2 Stress-strain curves for composites to added in MA-PP as a compatibilizer.

Development of New Natural Polymer-based Wood Adhesives: Effects of glucose addition on film and bonding properties of chitosan

Ayako Ishikawa

Laboratory of Sustainable Materials, RISH, Kyoto University

【Introduction】 Recent adhesives used in wood products are derived from petroleum resources. These adhesives contain organic compounds which are harmful for human health and environment. Therefore, the development of environmentally friendly wood adhesives derived from biomass resources is required. Chitosan which is a deacetylated of chitin is an abundant polysaccharide on Earth. It is known that, chitosan have good dry and wet bond strengths but have poor bond strength in dilute acid solution. Recently, it was reported that glucose-added chitosan film was almost insoluble in dilute acetic acid solution.

In this study, the physical and mechanical properties of glucose-added chitosan films were evaluated by changing the molecular weight of chitosan and the addition amount of glucose. In addition, the detailed bonding properties of glucose-added chitosan were investigated.

【Materials and Methods】 Chitosan powder (Molecular weight: 35000～350000, degree of deacetylation 70-80%) and glucose were used. In film preparation, chitosan (0.5 g) and glucose were dissolved in 1% acetic acid solution. The weight ratios of chitosan and glucose were adjusted to 10:0, 9:1, 8:2, 5:5, and 3:7. After removal of air in vacuo, the solution was poured into a plate, dried in an oven at 50˚C, and washed thoroughly to yield chitosan films. The films were examined for weight increase, color, free amino groups, tensile strength, solubility in water and in 5% acetic acid, and thermal properties. To evaluate the bond strength , three-ply plywoods (size 30 × 30 cm) were prepared using rotary-peeled lauan (*Shorea spp.*) veneers of 1.6 mm thickness. When chitosan and glucose were used as an adhesive, they were dissolved in 1% acetic acid solution. The hot-press temperature and pressure were 130˚C and 1 MPa, respectively. The total pressing time was 15 min. A normal, water immersion and repeated boiling tests were performed based on JIS K 6851. Resistance to dilute acetic acid was also measured.

【Results and Discussion】 In film properties, the tensile strength of pure chitosan films increased with increasing the molecular weight. The all films were almost insoluble in water, but soluble in 5% acetic acid solution. When glucose was added to chitosan, 10wt% glucose addition for a low molecular weight chitosan was effective for the tensile strength. Acid resistance developed by addition of >10wt% glucose regardless of the molecular weight of chitosan. 10wt% addition of glucose for low molecular weight was effective for the enhancement of film properties.

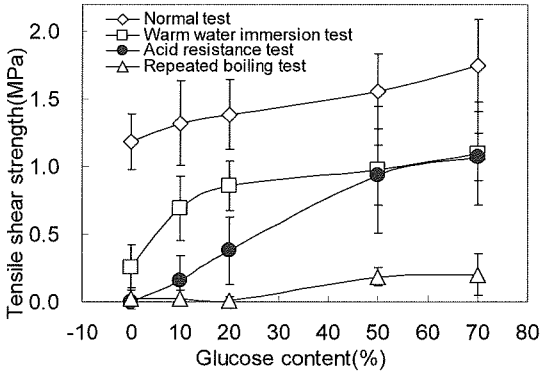

Fig. 1 Tensile strength of 3-ply plywood glued with chitosan and glucose

Fig. 1 shows the bond strength of 3-ply plywood glued with chitosan (M.W. 35000). As a whole, the bond properties were improved by addition of glucose. In the case of high molecular weight chitosan, the improvement of bonding properties was hardly observed. It was clarified that 50wt% addition of glucose for low molecular weight chitosan was effective for the improvement of the bonding properties of chitosan.

Development of floor system using Japanese cedar plank

Munekazu Minami

Wooden residential house is popular in Japan, while the percentage of using domestic lumber has been less than 30%. Recently, however, a new trend using regional lumber in urban area has been getting popular. It is pointed out that one of the features is called as the "exposed ceiling system". This is the system composed of planks with about 40mm thickness processed tongue-groove joint and completed by screwing them on beams. It is a good system on the point of an excellent design and workability that structure has also function of finishing. However, the shear resistance factor (SRF) has not been estimated and it is considered current method has a difficulty for achieving high SRF because of the slip between planks.

In this research, H-shaped fastener was developed for improving in-plane stiffness by preventing slip deformation between the planks at the initial stage so as to enhance SRF of this floor system. This fastener was designed as press-in type and to be easily driven into plank at construction site without harming the appearance of timber planks.

Full scaled shear test was performed by employing such floor test specimens of 1820 mm width, 2730mm height, as two typed current methods; i.e., hiding toe-screwed type in groove and flat-screwed type at the plank surface, as well as improved system with H-shaped fastener. Cyclic loading for each specimen was performed three times in each peak deformation. As a result, SRF of the current method was 0.6 and 0.8 respectively, while that of the improved system with one piece of H-shape fastener per 0.91m in one plank was 1.64 as shown in Table1.

Table 1 Test results and the estimated SRF.

Type of specimen			Toe screwd type	Sinked floor type	Flat screwed type	n-plane fastener typ
			T	S	F	FH
(1)	Py	(kN)	2.92	3.76	4.12	6.62
(2)	$Pu*0.2*\sqrt{(2\mu-1)}$	(kN)	2.19	2.46	2.96	5.87
(3)	$2/3(P\max)$	(kN)	4.69	5.65	5.80	8.03
(4)	$P1/150$	(kN)	2.28	2.24	2.92	5.84
Po (kN)			2.19	2.24	2.92	5.84
S.R.F(Shear Resistance Factor)			0.61	0.63	0.82	1.64

The improvement of single-braced shear wall system

Satoru Murakami

In Japanese conventional wooden residential houses, braced shear wall is one of the most popular shear walls. However, the strength of single-braced shear wall is different when the brace is subjected to compression and when subjected to tension. Therefore, two different directions of single-braced share walls have to be arranged in series, which has been one of the restrictions for structural designing of houses. The main reason of difference in strength between compression and tension was poor performance of brace connection, which tends to be composed of insufficient quantity and quality of fasteners in many cases. On the other hand, when compression is applied to the brace between sill and beams, single-braced shear wall could show higher strength performance, with a support by supplemental columns. In consequent, the strength of the braced shear wall when the brace member was subjected to compression was about twice as much as the case of tension.

The objective of this research is to develop a single-braced shear wall system, which has same performance both in tension and compression, and simultaneously has a shear resistance factor (SRF) of 3.0. For this aim, it is considered that the end connection of brace has to be progressed in tensile strength. In this research, two kinds of improvements were introduced on the end joint of brace.

First, a new LVL was introduced to make the variation of the strength of the brace joint lower. This LVL product is made of alternately laminating two different species of tropical wood; rubber wood *(Hevea brasiliensis)* and falcata (*Paraserianthes falcataria*). Secondly, the screw, which is used on the hardware to fasten the brace, was improved so as to have optimum diameter and material character to carry the load. Then the shear wall tests were performed to verify the performance of improved brace system.

LVL made of rubber wood and falcata can make the variation of the strength of the brace joint lower, and it made it possible to improve the tensile property of that. The developed screw showed high shearing strength and deformation performance. The shear wall evaluation test was done based on these results. In consequent, performances higher than a share resistant factor of 3.0 in tension and compression could be obtained in LVL types as shown in Table1.

Table 1. Evaluation test results

	Compression				Tension			
	Douglas fir		LVL		Douglas fir		LVL	
	Ave	Lower limt	Ave	Lower limit	Ave	Lower limit	Ave	Lower limit
Pmax	18.6	17.4	18.0	16.4	11.2	11.1	13.3	13.1
Py	11.5	10.8	10.5	9.8	6.2	6.0	7.6	7.0
(0.2/Ds)· Pu	8.9	8.6	6.6	5.9	5.5	4.4	7.5	7.2
2/3Pmas	12.4	11.6	12.0	10.9	7.5	7.4	8.9	8.7
P1/120	9.1	8.6	7.1	6.9	8.6	8.4	8.0	7.7
SRF	4.8		3.3		2.4		3.9	

Study on active mitigation of spacecraft charging in the Earth's polar region via three-dimensional particle-in-cell simulations

Koujirou Imasato
Laboratory of Computer Simulations for Humanospheric Science, RISH, Kyoto University

We studied the active mitigation of spacecraft charging in the Earth's polar region by performing three-dimensional Particle-In-Cell (PIC) simulations. In the Polar Earth Orbit (PEO), spacecraft charging occurs due to the aurora electrons impinging to the spacecraft surface along the magnetic field line. In such a situation, differential charging can occur between the solar panels made of dielectric materials and the conducting part of spacecraft. If this differential charging exceeds a threshold, discharge can occur and cause anomalies of spacecraft power system. In order to mitigate the spacecraft charging, active plasma emission from a plasma contactor device onboard spacecraft is one of the effective methods. However, the mitigation process has not been clearly understood in terms of spacecraft-plasma interaction. We investigated the mitigation process of the spacecraft charging in PEO by performing three-dimensional electrostatic PIC simulations. We first investigated the spacecraft charging process in the PEO environment. The floating potential of spacecraft becomes negative with respect to the plasma potential and the potential is determined when the amount of aurora electron flux and that of the background ion flux becomes equal. We also confirmed that the charging of the conducting part of spacecraft depends on the energy of aurora electrons while the differential charging at the solar panels depends on the direction of aurora electron flow.

We next investigated the charging mitigation of spacecraft in PEO by means of plasma release. In the case of electron release, negative potential of spacecraft surface including dielectric part basically increases up to the plasma potential. However, the electron release from the conducting surface cannot reduce the amount of the charge accumulated on the solar panel. To mitigate the negative charging on the solar panel, we performed ion release along with electrons from the contactor. In addition to the mitigation of conducting part of spacecraft by electron release, it turned out that negative charges on the solar panel are neutralized by the released ions. We also examined the dynamics of released plasma in terms of acceleration by sheath electric field and the influence of geomagnetic field. By considering the results obtained in the simulations, we discussed the effective condition of plasma release for the charging mitigation. We found that release of electrons with low energy and high-density along the geomagnetic field is the most effective for the charging mitigation in PEO. The analysis and discussion in the present research will be beneficial for the future design of plasma contactor device.

REFERENCES

[1] Garrett, H. B. and A. C. Whittlesey, Spacecraft charging, an update, IEEE Trans. Plasma Sci., vol. 28, no. 6, (2000), pp. 2017–2028.
[2] Rabin, A. G.: Spacecraft charging in the supra-auroral region, IEEE Transactions on Nuclear Science, Volume 36, Issue 6, Dec (1989), pp.2015 – 2020.
[3] Hastings, D. E.: Theory of plasma contactors used in the ionosphere, J. Spacecr. Rockets, 24, 3, (1987), pp.250-256.
[4] Usui, H., H. Matsumoto, M. Yasugi, and Y. Omura: PIC simulations of spacecraft charging and its neutralization process by plasma emission, Advances in Space Research, Vol.34, Issue 11, (2004), pp.2437-2440.

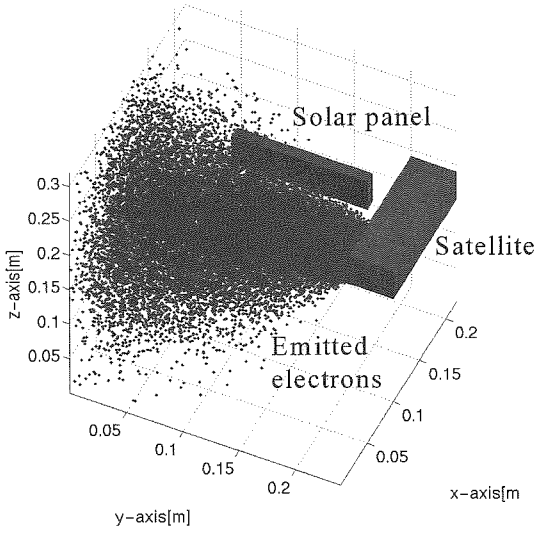

A snapshot of spatial distribution of electrons emitted from the satellite

Development on an outdoor model of microwave power transmission with a software retrodirective system

Takahiro Hirano
Research Institute for Sustainable Humanosphere, Kyoto University

Microwave power transmission is a useful way to send electric power from place to place. We can transmit electric energy wherever we want by microwave. Accurate beam direction control is important for microwave power transmission. One of the ways for the accurate beam direction control is a software retrodirective system.

In the software retrodirective system, firstly we estimate DOA (Direction of arrival) and transmit microwave to the direction. We developed software retrodirective system to make outdoor microwave power transmission experiments.

First, we conducted experiments to estimate DOA in an anechoic chamber. We sent a pilot signal from a patch antenna to power transmitting site. The frequency of the pilot signal was 5.815GHz. We received it by four patch antennas and calculated the DOA. The distance between the transmitter to the receiver was 3.79 meters long. Errors of the DOA estimation were less than 1.2 degree. We successfully estimated the DOA with high accuracy.

Second, we conducted experiments about microwave power transmission with a software retrodirective system. We used 16 patch antennas for a power transmitting part and one for a receiving part. The frequency was 2.46GHz. We used four patch antennas for a DOA estimating part and one for a transmitting part. The frequency was 5.815GHz. We changed DOAs and transmit microwave to the estimated directions. Receiving power is ideally constant in any directions. The results of the receiving power were nearly constant in any directions. The difference of the receiving power was under 2dB. We realized accurate microwave power transmission with the software retrodirective system.

Finally, we considered improvement parts of our system. Two important points are necessary to be improved. One is computational speed of the DOA estimation, the other is noise durability about pilot signal. To solve these problems, we proposed DOA estimation with Fourier Transform and using a Spread Spectrum signal for the pilot signal.

Research on a fast method of phase control process for microwave power transmission

Hua Zhengpeng
Research Institute for Sustainable Humanosphere, Kyoto University

People have paid more and more attentions to SPS (space power satellite). One of the most important issues of MPT (microwave power transmission) system in the SPS is highly effective power transmission. Since there is phase difference of the microwaves between different antennas, the microwaves from different antennas will offset each other. The concept of phase synchronization between antennas is put forward. This research is based on a fast phase control method which is called parallelization method.

Firstly, we introduce a phase control method which is mostly used in a MPT system. Then we compare this method with a parallelization method which we researched.

Secondly, we conducted certification experiments with one signal generator and two signal generators by using the parallelization method. The error of the experiments with one signal generator was about 1.4 degrees, after using an approximation straight line method to eliminate the error caused by the phase difference between two signal generators, the error of the experiments with two signal generators was 3.7 degrees.

At last we developed a phase control feedback system, this feedback system can make the phases of two signal generators synchronous. The error was less than 4 degrees. We conducted wireless experiments to test the feedback system. In the wireless environment, the feedback system could control the phase difference between two signals effectively. We found that the power at the receiving antenna got bigger after the phase difference was controlled by the feedback system between two antennas. Therefore the effectiveness of this feedback system was confirmed.

Develop1nent of 81na11 and high power amplifiers for an active integrated phased array antenna

Shigeaki Kawai
Research Institute for Sustainable Humanosphere, Kyoto University

An AIPAA (Active Integrated Phased Array Antenna) is a wireless transceiver with feature of small in size, light in weight and beam control. For its compactness and functionality, development of AIPAA system is expected in fields of a mobile communication system and a wireless power transmission system. For practical use of the AIPAA, cost reduction and size reduction of components are necessary. In these reasons, small high power and low-cost microwave circuits for the AIPAA are needed. The AIPAA consists of antennas, amplifier, phase shifter and other circuits. The objective of the present study is development of small and high power amplifiers for the AIPAA.

Small and high power 5.8GHz band amplifier circuit for the AIPAA were designed and fabricated. A driver amplifier is designed with GaAs HEMT. Its P_{1dB} (output power at 1dB gain compression point) was 7dBm with gain of 13dB. A high power two-stage amplifier circuit was designed and fabricated with high power GaAs FET. Its maximum output power is 31dBm (1.3W) at 5.8GHz with gain of 13dB. For compactness of amplifiers, a creased circuit substrate was considered. The loss in the creased circuit substrate was smaller than 0.4dB at 5.8GHz. The high power two-stage amplifier was bended with creased circuit substrate technology. It is proved that the creased circuit substrate is applicable to amplifier circuits. This method is applied to size reduction of high power AIA transmitter. In terms of downsizing amplifier circuits and cost reduction, MMIC (Microwave Monolithic Integrated Circuit) technology is effective. Two-stage amplifier was designed with FET chip for consideration of high power MMIC amplifiers. Its P_{1dB} was 27dBm with gain of 23dB. MMIC amplifier for 5.8GHz band was designed and computed its characteristics. Its P_{1dB} is 27.5dBm with gain of 31.5dB. The size of MMIC is 3mm x 3.5mm. MMIC amplifiers for 14GHz band were also designed and fabricated for high frequency AIPAA. With these circuits, a structure of small AIPAA was considered. Its thickness became smaller than 2.5cm.

Development of compact phase shifters with a Low Temperature Co-fired Ceramics substrate for an active integrated phased array antenna

Takeshi Yamamoto
Research Institute for Sustainable Humanosphere, Kyoto University

In recent days, various radio applications are allocated in microwave frequency bands. Furthermore, a wireless power transmission system with microwave is being studied. It is necessary to make the microwave transmission system smaller in size and lighter in weight for low cost. Hence, we propose an AIPAA (Active Integrated Phased Array Antenna) system, which is composed of patch antennas and microwave circuits such as amplifiers, phase shifters and power dividers. In this AIPAA system, the beam direction can be controlled electrically by changing microwave phase with phase shifters. The objective of the present study is to develop compact phase shifters for an AIPAA system.

Digital phase shifters for an AIPAA were designed and fabricated with a LTCC (Low Temperature Co-fired Ceramics) substrate. By using the LTCC technology in the phase shifter, small-sized and thin multi-layered phase shifters were realized. 4-bit switched-line type phase shifters with FET switches in 5.8GHz-band are fabricated. Their size is 10.0mm x 13.0mm x 0.55mm. The insertion loss of 2-bit phase shifters in the fabricated 4-bit phase shifters was measured to be -4.9dB ~ -6.4dB. The phase shifters had phase error of less than 2.7° after changing lengths of open stubs connected to the circuits of phase shifters. Experiment results show that the phase differences between the outputs of two 2-bit phase shifters were -6.8° ~ +7.0°.

Thrust Production Mechanism of Magnetic Sail Spacecraft with Superconducting Coil

Yuichiro Minami
Laboratory of Space Radio Science, RISH, Kyoto University

In the past decades, a lot of new propulsion system concepts for deep space missions were proposed and intensively investigated. One of them is called magnetic sail propulsion. The thrust of magnetic sail is generated, by utilizing the interaction between the plasma-flow solar wind and an artificial magnetic field produced around the spacecraft. It can be said that the solar wind energy is converted to the thrust of magnetic sail, which generates continuous high thrust in the outward radial direction from the sun to possibly achieve short flight-time transfer to planets in the solar system.

The first magnetic sail concept was proposed by Zubrin and extended by Winglee by introducing the plasma injection to inflate the artificial magnetic field. In order to obtain a continuous and high thrust, the use of a superconducting coil for generating the artificial magnetic field is appropriate, since a strong and continuous electric current can be maintained in superconducting materials without heat loss. In this study, we focus on such superconducting characteristics as well as coil design parameters, and evaluate the thrust characteristics of magnetic sail spacecraft.

First, two-dimensional analytical method for magnetic sail thrust model was introduced by extending that by Spreiter and Briggs for the Earth's magnetosphere in the solar wind. In the proposed method, the boundary electric currents and the induced magnetic field around the coils are used to obtain the thrust of magnetic sail. With this method, we investigate the thrust characteristics of magnetic sail spacecraft taking the coil design parameters into account. Then, the effect of superconductivity on the produced thrust magnitude is evaluated by comparing the two-dimensional analytical model with the results obtained by the magnetohydrodynamic simulation. Finally, in the three-dimensional model, the quantitative relation between the thrust and coil parameters (i.e., dimension and mass) are discussed.

REFERENCES

[1] H. Yamakawa, I. Funaki, Y. Nakayama, K. Fujita, H. Ogawa, S. Nonaka, H. Kuninaka, S. Sawai, H. Nishida, R. Asahi, H. Otsu, and H. Nakashima, "Magneto Plasma Sail: An Engineering Satellite Concept and its Application for Outer Planet Missions," Acta Astronautica, Vol. 59, No. 8-11, 2006, pp. 777-784.

[2] I. Funaki, H. Kojima, H. Yamakawa, Y. Shimizu, and Y. Nakayama, "Laboratory Experiment of Plasma Flow around Magnetic Sail", Astrophysics and Space Science, Vol.307, No.1-3, 2007, pp.63-68.

Development of highly-efficient microwave wireless charging system for electric vehicle

Junichiro Kojima
Laboratory of Space Radio Science, RISH, Kyoto University

Our research group has been studying on wireless power transmission system and applying this system for charging an electric vehicle these days. To charge an electric vehicle, microwave power is transmitted from the slot antennas on the ground to the antennas called rectennas on the bottom of the vehicle. Rectennas receive microwave and rectify it to DC power and this DC power is stored in capacitors. The objective of the present study is to improve charging efficiency. We introduced following three new devices.

First, we improve slot antennas. Characteristics of slot antennas get worse near some substances such as metal. In the conventional study, slot antennas used to be designed in free space, in this study, designed under rectennas instead so that slot antennas would be optimized in this charging environment and radiation efficiency goes up to 99.8%, 5.4% higher than that designed in free space.

Second, we downsize rectifiers of rectennas and improve their efficiencies. Rectifiers are composed of diodes, λ/4length microstriplines, output stubs and Wilkinson dividers. According to the results of experiments, longer output stubs make these rectifiers run with high efficiency even if microstriplines are shorter than λ/4. Owing to this characteristic, we succeed in downsizing rectifiers. Besides, last year our research group found that appropriate output phases of Wilkinson dividers result in higher efficiencies of rectifiers. Taking advantage of this, rectifiers come to run with higher efficiency up to 58% at 20W input.

Third, we introduce DC-DC converter. Input impedance of capacitors changes associated with their voltages, on the other hand, output impedance of rectennas should be stable to make them run with high efficiency. DC-DC converter between rectennas and capacitors keep output impedance of rectennas stable.

These three devices lead to the improvement of charging efficiency. As a result, charging efficiency from waveguide to capacitor goes up to 22%, 6% higher than that of last experiment.

REFERENCES

[1] Tetsuya Miyagawa, Development of a small and high power rectenna for a wireless power distribution system in a building (in Japanese), Master thesis of Kyoto University, 2006